Enteroendocrine progenitor cell enriched miR-7 regulates intestinal epithelial proliferation in an Xiap-dependent manner

Ajeet P. Singh, Yu-Han Hung, Michael T. Shanahan, Matt Kanke, Alessandro Bonfini, Michael K. Dame, Mandy Biraud, Bailey C.E. Peck, Oyebola O. Oyesola, John M. Freund, Rebecca L. Cubitt, Ennessa G. Curry, Liara M. Gonzalez, Gavin A. Bewick, Elia D. Tait-Wojno, Natasza A. Kurpios, Shengli Ding, Jason R. Spence, Christopher M. Dekaney, Nicolas Buchon, Praveen Sethupathy

PII: S2352-345X(19)30156-0
DOI: https://doi.org/10.1016/j.jcmgh.2019.11.001
Reference: JCMGH 543

To appear in: *Cellular and Molecular Gastroenterology and Hepatology*
Accepted Date: 7 November 2019

Please cite this article as: Singh AP, Hung Y-H, Shanahan MT, Kanke M, Bonfini A, Dame MK, Biraud M, Peck BCE, Oyesola OO, Freund JM, Cubitt RL, Curry EG, Gonzalez LM, Bewick GA, Tait-Wojno ED, Kurpios NA, Ding S, Spence JR, Dekaney CM, Buchon N, Sethupathy P, Enteroendocrine progenitor cell enriched miR-7 regulates intestinal epithelial proliferation in an Xiap-dependent manner, *Cellular and Molecular Gastroenterology and Hepatology* (2019), doi: https://doi.org/10.1016/j.jcmgh.2019.11.001.

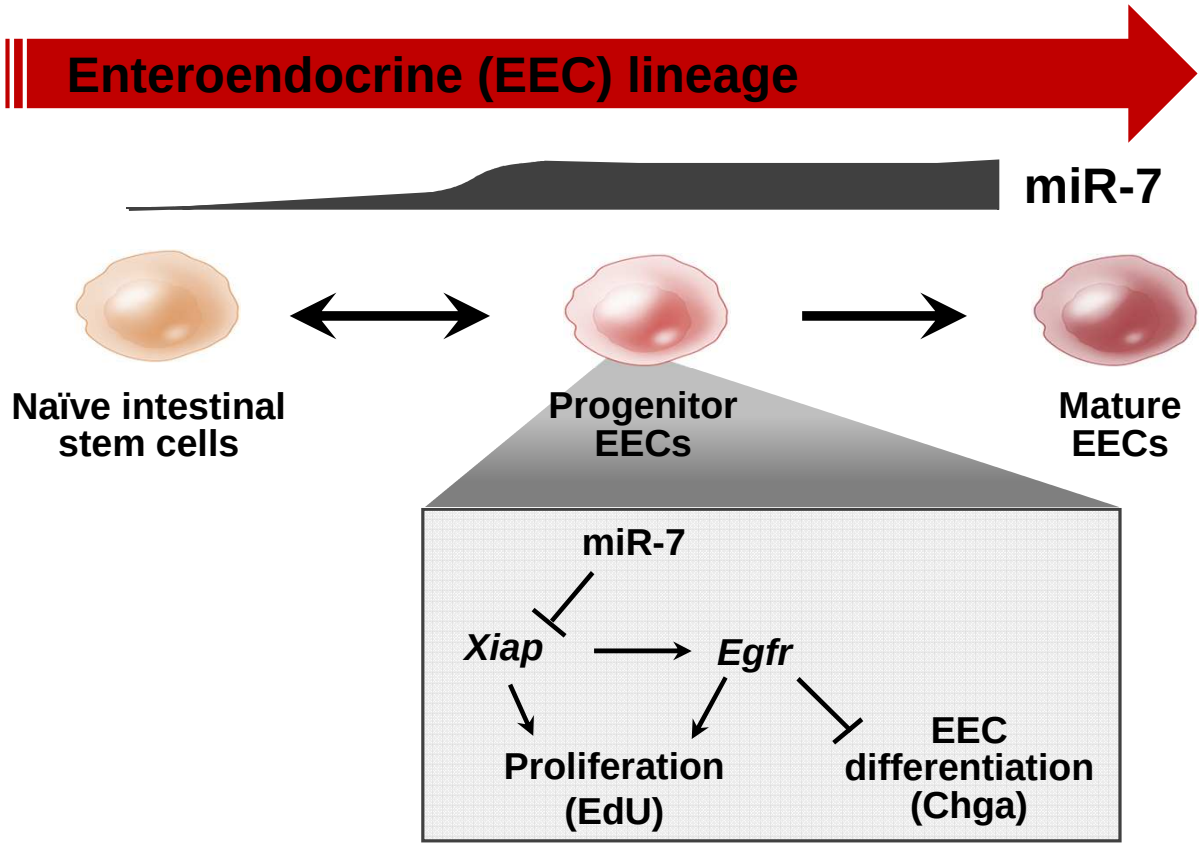

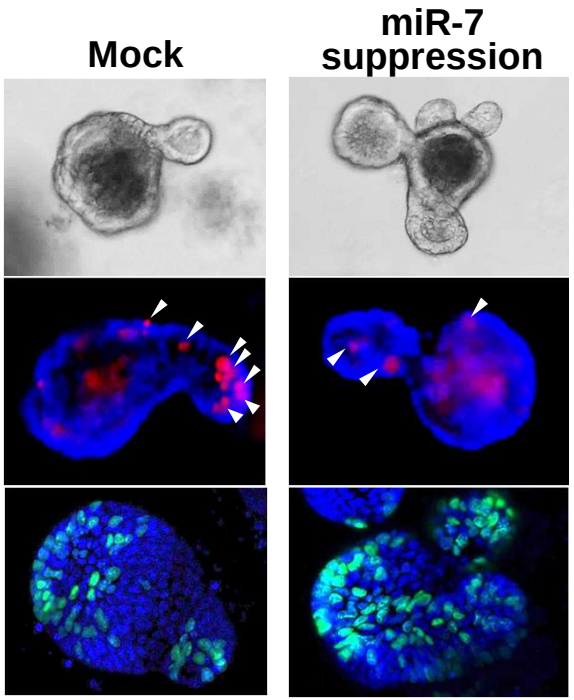

cmgh CELLULAR AND MOLECULAR GASTROENTEROLOGY AND HEPATOLOGY

Enteroendocrine progenitor cell enriched miR-7 regulates intestinal epithelial proliferation in an Xiap-dependent manner

Short title: miR-7 regulates intestinal proliferation via Xiap

Authors: Ajeet P. Singh[1,*], Yu-Han Hung[1,*], Michael T. Shanahan[1], Matt Kanke[1], Alessandro Bonfini[2], Michael K. Dame[3], Mandy Biraud[4], Bailey C.E. Peck[5], Oyebola O. Oyesola[6], John M. Freund[7], Rebecca L. Cubitt[1], Ennessa G. Curry[8], Liara M. Gonzalez[7], Gavin A. Bewick[9], Elia D. Tait-Wojno[6], Natasza A. Kurpios[10], Shengli Ding[8], Jason R. Spence[3], Christopher M. Dekaney[4], Nicolas Buchon[2], and Praveen Sethupathy[1]

[1]*Department of Biomedical Sciences, College of Veterinary Medicine, Cornell University, Ithaca, NY, USA*

[2]*Cornell Institute of Host-Microbe Interactions and Disease. Department of Entomology, Cornell University, Ithaca, NY, USA*

[3]*Department of Cell and Developmental Biology, University of Michigan, Ann Arbor, MI, USA*

[4]*Department of Molecular Biomedical Sciences, North Carolina State University, Raleigh, NC, USA*

[5]*Department of Surgery, University of Michigan, Ann Arbor, MI, USA*

[6]*Baker Institute of Animal Health and Department of Microbiology and Immunology, Cornell University, Ithaca, NY, USA*

[7]*Department of Clinical Sciences, North Carolina State University, Raleigh, NC, USA*

[8]*Department of Cell Biology and Physiology, School of Medicine, University of North Carolina, Chapel Hill, NC, USA*

[9]*Diabetes Research Group, School of Life Course Sciences, Faculty of Life Sciences and Medicine, King's College London, London, UK*

[10]*Department of Molecular Medicine, College of Veterinary Medicine, Cornell University, Ithaca, NY, USA*

**These authors contributed equally.*

Grant support: 1-16-ACE-47 ADA Pathway to stop Diabetes Research Accelerator (awarded to P.S.); C30293GG Empire State Stem Cell Fund (awarded to Y.-H. H.); IOS-1656118 and IOS-1653021 National Science Foundation (awarded to N.B.); U01DK103141 NIDDK/NIH and U19AI116482 NIAID/NIH (awarded to J.R.S.); R01DK100508 NIDDK/NIH (awarded to C.M.D.); EASD and JDRF project grants (awarded to G.A.B.); K01OD019911-01A1 Special Emphasis Research Career Award/NIH (awarded to L.M.G.); R01AG041198 NIA/NIH (awarded to S.D.).

Abbreviations: enteroendocrine cell, EEC; microRNA 7, miR-7; intestinal stem cell, ISC; Upper side population, USP; Lower side population, LSP; high-fat diet, HFD; locked nucleic acid, LNA; scramble, scr.

Correspondence: Praveen Sethupathy, Address: Department of Biomedical Sciences, Cornell University, Ithaca, NY, Email: pr46@med.unc.edu, Phone: 607-253-3214

Disclosures: The authors declare no competing interests.

Author contributions: A.P.S. and Y.-H.H. contributed to study design and were involved in all of the assays and data collection for the experiments done in the mouse system. A.B. and N.B. carried out the assays for all fruit fly experiments. M.K. performed all bioinformatic analyses. M.T.S. and S.D. contributed to experimental design and histology. M.T.S., B.C.P., and E.G.C. contributed to cell sorting and mouse enteroid experiments. M.K.D. and J.R.S. carried out experiments in human intestinal organoids. M.B. and C.M.D. performed cell sorting from the Defa6-Cre-tdTomato line. J.M.F. and L.M.G. carried out experiments in porcine enteroids. G.A.B. contributed to cell sorting from the Pyy-GFP line. O.O.O and E.D.T. helped sort and analyze tuft cells. R.L.C. and N.A.K. helped established the Prox1-GFP colony. P.S. initiated the project, secured funding, led the experimental designs, and supervised the study. A.P.S., Y.-H.H., and P.S. wrote the manuscript. All of the authors made important intellectual contributions to the experiments and discussion.

Word count: 4300

Synopsis

It was recently shown that progenitors of enteroendocrine cells (EECs) contribute to intestinal epithelial growth, but the underlying mechanisms remain poorly understood. We uncover the role of EEC-progenitor enriched miR-7 in regulating intestinal epithelial growth via Xiap and Egfr signaling.

Abstract

Background & Aims: The enteroendocrine cell (EEC) lineage is important for intestinal homeostasis. It was recently shown that EEC progenitors contribute to intestinal epithelial growth and renewal, but the underlying mechanisms remain poorly understood. MicroRNAs are under-explored along the entire EEC lineage trajectory, and comparatively little is known about their contributions to intestinal homeostasis. **Methods:** We leverage unbiased sequencing and eight different mouse models and sorting methods to identify microRNAs enriched along the EEC lineage trajectory. We further characterize the functional role of EEC progenitor-enriched miRNA, miR-7, by *in vivo* dietary study as well as *ex vivo* enteroid in mice. **Results:** First, we demonstrate that miR-7 is highly enriched across the entire EEC lineage trajectory and is the most enriched miRNA in EEC progenitors relative to Lgr5+ intestinal stem cells. Next, we show *in vivo* that in EEC progenitors miR-7 is dramatically suppressed under dietary conditions that favor crypt division and suppress EEC abundance. We then demonstrate by functional assays in mouse enteroids that miR-7 exerts robust control of growth, as determined by budding (proxy for crypt division), EdU and PH3 staining, and likely regulates EEC abundance also. Finally, we show by single cell RNA-sequencing analysis that miR-7 regulates *Xiap* in progenitor/stem cells and we demonstrate in enteroids that the effects of miR-7 on mouse enteroid growth depend in part on Xiap and Egfr signaling. **Conclusions:** This study demonstrates for the first time that EEC progenitor cell-enriched miR-7 is altered by dietary perturbations and that it regulates growth in enteroids via intact Xiap and Egfr signaling.

Key words: miR-7; enteroendocrine lineage; small intestine; enteroid; proliferation

Introduction

The intestinal epithelium is the most rapidly renewing tissue in the body. This feature is driven by crypt-based intestinal stem cells (ISCs), which exhibit self-renewal properties and are responsible for giving rise to all of the differentiated cell types in the absorptive (enterocyte) and secretory lineages (Paneth cell, tuft cell, goblet cell and enteroendocrine cells (EECs)) (1). So far, two distinct populations of ISCs have been defined: actively cycling ISCs (aISCs) at the base of the crypt and reserve/slowly cycling ISCs (rISCs) at the +4 position from the crypt base (2). More recently, though, several other intermediate cell populations, notably progenitors of EECs, have been shown to participate in the control of crypt behavior under certain conditions (3, 4).

EEC progenitors, which were thought to be fully committed to EEC differentiation, have recently been recognized to have proliferative potential and thereby contribute to the control of cell proliferation, crypt growth, and related behaviors (3, 4). A recent study identified Prospero homeobox protein 1 (Prox1) as a novel marker labeling intermediates in the EEC lineage and demonstrated that sorted Prox1+ cells are sufficient for establishing enteroids *ex vivo*. Despite this advance, much remains unknown about the mechanisms that control EEC lineage behavior. It is of substantial interest to map the molecular landscape of the cells in the entire EEC lineage trajectory in order to define the mechanisms that control intestinal epithelial cell proliferation, crypt division/growth, and/or EEC differentiation.

MicroRNAs (miRNAs) are prominent post-transcriptional regulators of growth and cell fate decisions in many organ systems and disease models (5, 6); however, very little is known about their role in the regulation of intestinal crypt behavior. In fact, it is not even known which miRNAs are expressed along the entire EEC lineage trajectory, particularly the EEC progenitors

or whether they are sensitive to perturbations that influence crypt division and/or EEC differentiation (7). In this study, using eight different reporter mice and several sorting methods, we profile miRNAs in several lineages of the small intestinal epithelium, identify miR-7 as the most highly enriched miRNA in EEC progenitors relative to Lgr5+ stem cells, show that miR-7 in EEC progenitors is among the most sensitive miRNAs to dietary conditions that favor crypt growth and reduced EEC abundance, and demonstrate through *ex vivo* functional studies and single cell analyses that miR-7 controls enteroid growth in part by regulation of Xiap.

Results

MiR-7 is the most enriched miRNA in EEC progenitors relative to Lgr5+ stem cells

In this study, we defined the enteroendocrine cell (EEC) lineage trajectory as the following: (i) Lgr5+ aISCs, (ii) Sox9-Low cells and Hopx+ cells that exhibit features of the EEC lineage, (iii) Prox1+ EEC progenitors, (iv) Sox9-High and lower side population (LSP) cells that represent a mixed population of rISCs and mature EECs, and (v) Pyy+ cells that represent mature EECs. To define the miRNA landscape across the EEC lineage trajectory, we first investigated Sox9-EGFP reporter mice (**Fig. 1A**). From the jejunal crypts of the Sox9-EGFP mice, we sorted and performed small RNA-sequencing analysis on four different epithelial cell populations enriched in enterocytes (Sox9-Negative), stem cells/EEC progenitors (Sox9-Low) (hereafter referred to as 'EEC progenitors'), transit amplifying cells (Sox9-Sublow), and mature EECs (Sox9-High), and demonstrated that each fraction is enriched for the expected markers (**Fig. 1B**). We then focused our analysis on the cell populations in the EEC lineage trajectory, Sox9-Low and Sox9-High. The small RNA-seq analysis identified a total of 187 miRNAs in these two populations. Of these, we found that only 8 miRNAs are enriched (>5-fold) in mature EECs (class A), 2 in stem/EEC

progenitors (class B), and 14 in both (class C) relative to unsorted intestinal epithelial cells (**Table 1**). Class A miRNAs represent candidate regulators of mature EEC function, class B miRNAs represent candidate regulators of EEC progenitor cell behavior, and class C miRNAs represent candidate regulators of both mature EEC function and EEC progenitor cell behavior. Notably, class C miRNAs include miR-7b, which has been previously extensively studied in the context of endocrine pancreatic development and function (8-15). miR-7 was also shown to be enriched in a specific subtype of mature EECs, cholecystokinin-producing EECs (16), and also in enterochromaffin cell-derived tumors (17); however, importantly, the expression pattern of miR-7 (or any other miRNA) across the entire EEC lineage trajectory has never before been reported.

Next, from the jejunal crypts of Lgr5-EGFP, Prox1-EGFP, and Hopx-CreERT2;Rosa26-tdTomato reporter mice (**Fig. 1A**), we sorted Lgr5+, Prox1+, and Hopx+ cells, respectively, and performed small RNA-seq to define miRNA profiles in each population (**Fig. 1C**). We found that the level of expression of miR-7a and miR-7b increases steadily along the EEC trajectory from Lgr5+ aISCs to Sox9-Low EEC progenitors to Sox9-High mature EECs, in contrast to other miRNAs such as miR-194 and miR-215, which are depleted in the EEC lineage and enriched in the non-EEC, absorptive lineage (Sox9-Sublow and Sox9-Negative) (**Fig. 1D**). We also found by qPCR that miR-7 is significantly enriched in Hopx+ cells (**Fig. 1E**), which have been shown previously to exhibit molecular features of EEC progenitors (18). Moreover, through small RNA-seq analysis we found that miR-7b is one of the top three miRNAs to be significantly enriched (>5-fold enrichment based on expression as measured by reads per million mapped to

183 miRNAs [RPMMM] and $P < 0.05$ by two-tailed Student's t-test) in Hopx+ cells relative to
184 Hopx- cells, further underscoring the potential importance of miR-7b in EEC progenitors.
185
186 To validate that the miR-7 family is enriched in EEC progenitors, we next performed side
187 population sorting of the intestinal epithelium and isolated the lower side population (LSP) and
188 upper side population (USP) of cells, which correspond to reserve intestinal stem cells (rISCs)
189 and aISCs, respectively (**Fig. 1A**). Consistent with the notion of overlapping identity between
190 rISCs and cell populations in the EEC lineage (18), we found that LSP cells exhibit molecular
191 features of mature EECs and EEC progenitors, including expression of *Chga* (**Fig. 1F**), and are
192 depleted for markers of aISCs, including *Lgr5* (**Fig. 1F**). RT-qPCR analysis showed that miR-7
193 is significantly enriched in LSP relative to both USP and Lgr5+ cells (**Fig. 1F**), confirming miR-
194 7 enrichment in cells with EEC progenitor features.
195
196 To cement the finding of miR-7 enrichment in EEC progenitors, we next turned our attention to
197 the Prox1+ cells sorted from the intestinal epithelium of Prox1-EGFP reporter mice (**Fig. 1A, C**).
198 Prox1 was recently shown to mark intestinal secretory progenitors with the capacity to either
199 differentiate to mature EECs or exhibit proliferative stem-cell like activity (4), and our small
200 RNA-seq analysis showed that the miRNA profile of intestinal epithelial Prox1+ cells most
201 closely resembles that of Hopx+ cells (rISCs/EEC progenitors) and Sox9-Low cells (EEC
202 progenitors) (**Fig. 1C**). We first demonstrated by qPCR that the traditional EEC lineage marker,
203 *Chga*, and miR-7 are significantly enriched in Prox1+ cells (**Fig. 1G**). Then, we analyzed the
204 small RNA-seq data and found that only ten miRNAs are >5-fold enriched in Prox1+ cells
205 relative to Prox1- cells (**Fig. 1H**). Several of these, including miR-7b, overlap with the class C

miRNAs defined in **Table 1**. Notably, among these ten miRNAs, we found that miR-7b is by far the most dramatically enriched (~41-fold) in Prox1+ EEC progenitors relative to Lgr5+ aISCs (**Fig. 1I**).

Prox1+ progenitor cells are thought to give rise not only to mature EECs but also to differentiated tuft cells. To determine whether miR-7 is truly enriched along the EEC lineage trajectory, or also highly abundant in tuft cells, we next measured miR-7 in mouse jejunal tuft cells (Epcam+/Siglecf+/Cd45- cells sorted from wild-type C57BL/6J mice), which are highly enriched as expected for the tuft cell marker *Dclk1* (**Fig. 1J**). This analysis revealed that miR-7 is >350-fold enriched in Sox-9 High EECs relative to Dclk1+ tuft cells (**Fig. 1J**). As a control, we also included Lyz1+ Paneth cells sorted from the Defa6-Cre;tdTomato line (**Fig. 1J**), and demonstrated that miR-7 is indeed significantly depleted in these cells relative to Sox9-High EECs (**Fig. 1J**). As additional validation, we sorted Pyy+ EECs from the jejunum of Pyy-EGFP reporter mice and found that miR-7 is >600-fold more highly expressed in Pyy+ cells than in tuft cells (data not shown). These findings provide strong support for the enrichment of miR-7 along the entire EEC lineage trajectory.

Taken together, these data define a clear EEC lineage trajectory (from Lgr5+ aISCs to mature EECs) miRNA signature for the first time and reveal that miR-7 is the most enriched miRNA in EEC progenitors compared to Lgr5+ aISCs.

MiR-7 expression in EEC progenitors, not mature EECs, is suppressed under conditions of increased intestinal crypt division and reduced EEC abundance

Several different types of environmental perturbations, including dietary modifications, have been reported to alter both crypt growth and EEC differentiation (19, 20). For example, high-fat diet (HFD) robustly increases intestinal crypt division (indicative of enhanced proliferation) and decreases EEC abundance in mice compared to low-fat diet (LFD) (20). Our above-described expression analysis demonstrated that miR-7 is highly expressed in Sox9-Low EEC progenitor cells (**Fig. 1D**), which exhibit both proliferative and differentiative capacity, but relatively low in Lgr5+ aISCs (**Fig. 1D**). If miR-7 is critical to the control of crypt division and/or EEC abundance, we reasoned that it may be modulated by HFD. To determine whether miR-7 is significantly altered by HFD, we performed a HFD study for 16 weeks, identical to the one previously described in Mah et al., 2014. First, we confirmed that HFD-fed mice exhibit a significant increase relative to LFD-fed mice in body weight as expected (58.8% increase; $P = 1.271e-9$; LFD, $n = 8$; HFD, $n = 9$). Next, we showed by histomorphometry that crypt density, a marker of the rate of crypt division, is significantly elevated in the jejunum of HFD-fed mice (**Fig. 2A**). We also observed a significant increase in the number of EdU+ cells/crypt (proliferating cells) in jejunal crypts from HFD-fed mice (**Fig. 2B**). Finally, we demonstrated by immunofluorescence (IF) that HFD-fed animals exhibit significantly lower Chga+ cell/villus count, indicative of reduced EEC number (**Fig. 2C**).

To determine whether the EEC progenitor enriched miR-7 is associated with this hyper-proliferative phenotype, we next performed small RNA-seq in sorted Sox9-Low cells (EEC progenitors) from the jejunal epithelial tissue of both LFD- and HFD-fed mice (**Fig. 2D**). Principal component analysis (PCA) on miRNA profiles showed clear separation of LFD- and HFD-fed mice (**Fig. 2E**) and differential miRNA expression analysis identified 15 miRNAs (7

up, 8 down) in Sox9-Low cells altered by more than 2-fold (**Fig. 2F**). Notably, the down-regulated group of miRNAs includes the EEC lineage-enriched miR-7b (**Fig. 2G**. In addition, the downregulation of miR-7b by the dietary perturbation appears specific to EEC progenitors, as it is downregulated by HFD only in Sox9-Low (EEC progenitors) but not in Sox9-High (mature EECs) (**Fig. 2H).** This finding indicates that miR-7 is suppressed in EEC progenitors under physiologic conditions that promote crypt division and reduce EEC abundance in the intestinal epithelium.

Genes upregulated in EEC progenitors under conditions of increased crypt division are enriched for predicted targets of miR-7

Given that HFD alters miR-7 in Sox9-Low (EEC progenitors) but not Sox9-High cells (mature EECs) (**Fig. 2G**), we next performed RNA-seq in sorted Sox9-Low cells from the jejunal epithelial tissue of both LFD- and HFD-fed mice (**Fig. 2D**). PCA on gene expression profiles showed clear separation of LFD- and HFD-fed mice (**Fig. 2I**) and differential expression analysis identified nearly 1700 significantly (adjusted $P < 0.05$) altered genes (410 up, 1279 down) (**Fig. 2J**). After multiple testing correction, the genes up-regulated by HFD are most significantly enriched in the Pparδ transcriptional network (Enrichr KEGG, P=9.89e-6), including genes involved in fatty acid oxidation (**Fig. 2K**), which is consistent with the finding from a recent study in the colon after a much longer high-fat diet regimen (21). In the HFD condition, we also found that several genes involved in crypt division and enterocyte differentiation are significantly up-regulated whereas genes that encode transcription factors that drive EEC maturation are significantly down-regulated (**Fig. 2K**), which is in line with the observed cellular phenotypes (**Fig. 2A-C**). Using the bioinformatic tool miRhub (22) , we showed that upregulated

genes are significantly enriched for predicted target sites of only one downregulated miRNA, miR-7 (**Fig. 2L**). This shows that genes up-regulated in EEC progenitors under conditions of increased intestinal epithelial proliferation are over-represented for predicted targets of miR-7. Notably, among the upregulated genes is X-linked inhibitor of apoptosis (*Xiap*) (**Fig. 2M**), which encodes a protein that promotes crypt survival and growth. While *Xiap* has been reported as a direct target of miR-7 in the context of cervical cancer (23), it has never been reported previously in the small intestine. Indeed, the levels of *Xiap* and miR-7b are strongly inversely correlated in EEC progenitors across LFD- and HFD-fed mice (**Fig. 2N**).

MiR-7 controls intestinal epithelial growth

The above findings, most notably that miR-7 in EEC progenitors is strongly suppressed under conditions of increased crypt division and that the genes upregulated during increased crypt division are enriched for miR-7 predicted targets, led us to hypothesize that miR-7 may regulate crypt division. To test this hypothesis, we established three-dimensional enteroids from jejunal crypts of C57BL6/J mice and treated them with locked nucleic acid inhibitors against miR-7 (LNA-7) and compared to treatment with LNA-scramble control (LNA-scr) (**Fig. 3A**). RT-qPCR analysis showed that treatment with LNA-7 led to a robust suppression (~55-fold) of the miR-7 family in enteroids (**Fig. 3B**). Also, small RNA-seq analysis of LNA-7 treated enteroids revealed that miR-7 is suppressed by many orders of magnitude more than any other miRNA (**Fig. 3C, Table 2**), demonstrating the specificity of the effects of LNA-7 on miR-7 expression.

Brightfield imaging showed that treatment with LNA-7 (miR-7 loss-of-function) significantly increases enteroid budding, which is an *ex vivo* proxy for crypt division (24), relative to LNA-scr

and mock (no treatment) controls (**Fig. 3D, E**). We also confirmed this result in porcine enteroids (**Fig. 3F**). Furthermore, we demonstrated that LNA-7 treatment dramatically increases EdU+ cells/enteroid (**Fig. 3G**) and PH3+ cells/enteroid (**Fig. 3G, H**). Next, we performed complementary gain-of-function studies in mouse enteroids using miR-7 mimics. Our results showed that over-expression of miR-7 (**Fig. 3I**) suppresses budding (**Fig. 3J, K**) and leads to a reduction in PH3+ cells/enteroid (**Fig. 3J-L**), which is the opposite of what occurs upon inhibition of miR-7. These studies together demonstrate the functional role of miR-7 in the control of enteroid budding.

MiR-7 controls intestinal epithelial proliferation in Drosophila midgut in vivo

To determine whether this function of miR-7 is conserved beyond mammals, we turned to the fruit fly model (**Fig. 4A**). We first demonstrated that miR-7 is the most significantly reduced miRNA in the *Drosophila melanogaster* midgut during the well-documented hyper-proliferative response to infection by *Erwinia carotovora carotovora* 15 (*Ecc*15) (25) (**Fig. 4B, C**). In order to study miR-7 function specifically in proliferating intestinal epithelial cells, we over-expressed miR-7 (miR-7 OE) in esg+ cells of the midgut, which represent the stem/progenitor populations. We found that the number of PH3+ (proliferating) cells is dramatically reduced upon miR-7 over-expression in the background of *Ecc*15 infection compared to control (**Fig. 4D, E**), which demonstrates that miR-7 downregulation is required for the hyper-proliferative response to bacterial insult and that miR-7 is a key regulator of epithelial proliferative capacity in the midgut. While our focus is on mammalian miR-7, and while there are notable differences between fruit fly and mammalian gut tissue (for example, lack of well-established EEC progenitors in the fruit

fly gut), the results from the *Drosophila* experiments convey a remarkable evolutionary conservation of miR-7 function in the intestinal epithelium.

MiR-7 control of enteroid budding is dependent on intact Xiap

As mentioned previously, *Xiap* encodes a protein that promotes cell survival and growth, and it is an established direct target of miR-7 by 3' UTR reporter gene assays in a cancer cell context (23). However, the functional relevance of the miR-7:Xiap regulatory relationship has not been examined in a non-cancer context and definitely not in intestinal epithelial growth. To determine whether miR-7 regulates *Xiap* in enteroids, and to determine whether this regulation takes place in proliferating cells (stem/progenitors), we performed single cell RNA-seq (scRNA-seq) in mouse enteroids treated with either LNA-scr or LNA-7. We sequenced just enough cells to discern three clusters of different cell types, progenitor/stem, Paneth, and enterocyte (**Fig. 5A**). These cell clusters are enriched for markers that are known to be associated with each cell type (**Fig. 5B, C**). Notably, the signal for markers of proliferation increased in the progenitor/stem population after treatment with LNA-7 (**Fig. 5C**). Next, we focused on *Xiap* and found that its average level across all cells is significantly elevated by treatment with LNA-7 relative to LNA-scr (**Fig. 5D**). Moreover, the percentage of *Xiap*+ progenitor cells is ~2-fold increased by LNA-7 (~21%) relative to LNA-scramble (~10%) (**Fig. 5E**). In progenitor/stem cells, the fold-increase of *Xiap*+ cells after LNA-7 treatment is even greater (~3-fold, **Fig. 5F**). These results suggest that more progenitor/stem cells express *Xiap*, and at higher levels, after LNA-7 treatment. Although mouse enteroids are comprised of many differentiated cell types, most of which do not robustly express miR-7, human enteroids tend to retain a more stem/progenitor state in culture

342 (26). Therefore, to test miR-7 regulation of *XIAP*, we treated human enteroids with LNA-7,
343 which led to dramatic suppression of miR-7 and a significant increase in *XIAP* (**Fig. 5G**).
344
345 To determine whether miR-7 control of enteroid growth is mediated in part by regulation of
346 Xiap, we examined the effect of LNA-7 in mouse enteroids in the context of Xiap suppression.
347 Treatment of enteroids with GDC0152, an Xiap inhibitor, effectively reduced Xiap+ cells per
348 enteroid (**Fig. 5H**) and suppresses the budding phenotype (**Fig. 5I**). We then showed that
349 treatment with GDC0152 significantly blunts the effects of LNA-7 on Xiap+ cells/enteroid (**Fig.**
350 **5J**), budding (**Fig. 5K**), and PH3+ cells/enteroid **(Fig. 5L)**. These results convey that the effects
351 of miR-7 on enteroid growth are mediated at least in part through regulation of Xiap.
352
353 Xiap is known to promote Egfr (27). To evaluate further the dependency on Egfr, we next tested
354 the effect of LNA-7 in the context of direct Egfr suppression. We first demonstrated in mouse
355 enteroids that treatment with an oligonucleotide inhibitor of Egfr (Gapmer Egfr) down-regulates
356 *Egfr* mRNA levels by ~60% (**Fig. 6A**) and significantly reduces enteroid budding as expected
357 (**Fig. 6B, C**). Then we showed that treatment of enteroids with Gapmer Egfr significantly blunts
358 the pro-proliferative phenotype observed with LNA-7 alone or with Gapmer Control, as
359 determined by budding (**Fig. 6D, E**) and EdU staining (**Fig. 6E**). Also, we demonstrated that
360 *Egfr* suppression greatly blunts the hyper-budding phenotype in LNA-7 treated enteroids
361 compared to LNA-scr treated enteroids (**Fig. 6F**).
362
363 A previous study established that Egfr signaling can suppress EEC differentiation (28). Given the
364 finding that miR-7 function is dependent in part on Egfr signaling, we hypothesized that loss of

365 miR-7 may shift the balance of secretory progenitor cells toward proliferation and away from
366 EEC maturation. Indeed, in our scRNA-seq data from mouse enteroids, we found that LNA-7
367 treatment increases the proportion of Prox1+ cells (proliferative EEC progenitors) and decreases
368 the proportion of Chga+ cells (mix of EEC progenitors primed to differentiation and mature
369 EECs) in the progenitor population (**Fig. 6G, H**). To validate this observation, we showed that
370 treatment of enteroids with LNA-7 leads to a significant increase in Prox1-EGFP+ cells/enteroid
371 (**Fig. 6I**) and a significant decrease in Chga+ cells/enteroid (**Fig. 6J**). Taken together, these data
372 strongly suggest that EEC progenitor enriched miR-7, in part through Xiap and Egfr, controls
373 enteroid budding (proxy for crypt division) and may also be involved in the regulation of EEC
374 abundance (**Fig. 6K**).
375
376 **Discussion**
377 Although miRNAs are well-appreciated as regulators of cell division, growth, and differentiation
378 in many organ systems, their contributions in the intestinal epithelium remain largely unknown.
379 Recently, several studies have reported that EEC progenitors represent a plastic cell population
380 that can either drive the formation of mature EECs or exhibit stem cell-like proliferative capacity
381 (3, 4). Here, we have: (1) identified miR-7 as a highly enriched miRNA across the entire EEC
382 lineage trajectory, using eight different reporter mice, FACS, and small RNA-seq; (2) defined
383 miR-7 as the most enriched miRNA in EEC progenitors relative to Lgr5+ stem cells; (3)
384 demonstrated that miR-7 in the EEC progenitor population is dramatically suppressed under
385 physiological conditions of increased crypt division; (4) showed that miR-7 controls enteroid
386 budding and EEC progenitor cell behavior; and (5) showed that miR-7 function depends at least
387 in part on intact Xiap and downstream Egfr signaling. To our knowledge, this is the first report

388 of a miRNA enriched along the EEC lineage trajectory that exerts substantive control of enteroid
389 growth and likely EEC abundance. Although previously miR-7 has been reported to have roles in
390 specific cancer contexts (17, 29, 30), our study is the first to our knowledge to demonstrate that
391 miR-7 regulates intestinal growth under normal physiological conditions. It is noteworthy that
392 modest but significant changes in miRNA expression, similar to what we show for miR-7 in this
393 study, have been linked functionally to important phenotypes in numerous prior studies (31-33).
394
395 Although our data suggest that miR-7 has important roles in EEC progenitor cells, we also
396 cannot rule out functions in other stem/progenitor cell types. Also, though we have
397 demonstrated that manipulating miR-7 expression regulates intestinal epithelial proliferative
398 capacity, whether miR-7 controls the abundance of specific subtypes of mature EECs requires
399 future detailed investigation. In addition, we have observed downregulation of miR-7 only in
400 EEC progenitors but not in mature EECs upon HFD (**Fig. 2**), motivating the question of what
401 upstream mechanisms regulate miR-7 in this cell-type specific manner. A study in *Drosophila*
402 showed that Ato, the mammalian ortholog of which is Atoh1 (a known EEC lineage driver in
403 mouse), is upstream of miR-7 during development (34). Whether Atoh1 regulates miR-7 in the
404 mammalian intestinal epithelium and whether Atoh1 is responsible for the alteration of miR-7
405 expression upon HFD remain to be determined in the future.
406
407 Though mature EECs constitute only ~1% of cells in the intestinal epithelium, they are critical
408 for orchestrating proper responses to nutritional and microbial input in order to maintain energy
409 homeostasis and immune function (35-37). They are known to secrete many different kinds of
410 hormones that function through endocrine and paracrine signaling, and they are thought to be

major contributors to the immediate, weight-loss independent positive metabolic effects of bariatric surgery (38). Also, recent studies have implicated EECs in the gut-brain axis and the immune-endocrine axis through direct connection to enteric nervous system and surrounding immune cells, respectively (39). While changes in EEC abundance and/or function have been linked to a wide array of diseases including diabetes, inflammatory bowel disease, and psychiatric/neurologic disorders (40, 41), the key regulators of the EEC lineage remain incompletely characterized due in part to the rareness, high molecular heterogeneity, and plasticity of this cell population. In the present study, we uncovered the functional role of EEC lineage-enriched miR-7 particularly in regulating intestinal epithelial growth and also provided observations suggesting its role in regulating EEC abundance. The potential role of miR-7 in regulating EEC maturation and function warrants future studies.

In vivo loss-of-function studies of miR-7 is made extremely challenging by the fact that there are three different miR-7 paralogs in mice, miR-7a-1, miR-7a-2, and miR-7b. We believe the current study provides strong motivation to invest in the generation of an EEC progenitor cell-specific miR-7 triple-knockout mouse colony. These mice will be useful for future *in vivo* investigation of the role of miR-7 in intestinal epithelial proliferation and renewal under baseline conditions and in response to different perturbations that affect crypt behavior, including high-fat diet, pathogenic gastrointestinal infection, irradiation, or even bariatric surgery. Finally, we note that this study identifies several other miRNAs in addition to miR-7 that are enriched in the EEC lineage trajectory and altered under conditions of increased crypt budding. It will also be of great interest to investigate the role of these miRNAs too, in isolation and in conjunction with miR-7, in controlling the biology and pathophysiology of the crypt in the intestinal epithelium.

Acknowledgements

We would like to thank members of the Sethupathy laboratory and Susan Henning for helpful comments and feedback at various stages of the study, Dr. Richard Blumberg for permission to use the Defa6-Cre-tdTomato mice in this study, Dr. Zhao Li and the Greehey Children's Cancer Research Institute at University of Texas Health Science Center at San Antonio for small RNA library preparation and sequencing, Dr. Jen Grenier and the Cornell RNA-sequencing core facility for RNA-sequencing, the Cornell University and UNC Chapel Hill Flow Cytometry Core Facilities, the Cornell University East Campus Mouse Research Facility, and the following funding sources (1-16-ACE-47 ADA Pathway to stop Diabetes Research Accelerator, awarded to P.S.; C30293GG Empire State Stem Cell Fund, awarded to Y.H.; IOS-1656118 and IOS-1653021 National Science Foundation, awarded to N.B.; U01DK103141 NIDDK/NIH and U19AI116482 NIAID/NIH, awarded to J.R.S.; R01DK100508 NIDDK/NIH, awarded to C.M.D.; EASD and JDRF project grants, awarded to G.A.B.; K01OD019911-01A1, awarded to L.M.G.; and R01AG041198 NIA/NIH, awarded to S.D.).

Author contributions

A.P.S. and Y.-H.H. contributed to study design and were involved in all of the assays and data collection for the experiments done in the mouse system. A.B. and N.B. carried out the assays for all fruit fly experiments. M.K. performed all bioinformatic analyses. M.T.S. and S.D. contributed to experimental design and histology. M.T.S., B.C.E., and E.G.C. contributed to cell sorting and mouse enteroid experiments. M.K.D. and J.R.S. carried out experiments in human intestinal organoids. M.B. and C.M.D. performed cell sorting from the Defa6-Cre-

tdTomato line. J.M.F. and L.M.G. carried out experiments in porcine enteroids. G.A.B. contributed to cell sorting from the Pyy-GFP line. R.L.C. and N.A.K. helped established the Prox1-GFP colony. P.S. initiated the project, led the experimental designs, and supervised the study. A.P.S., Y.-H.H., and P.S. wrote the manuscript. All of the authors made important intellectual contributions to the experiments and discussion.

Materials and Methods

Animal models and diet study. The following transgenic reporter mice were utilized: female and male Sox9-EGFP (42), female Lgr5-EGFP (24), female Prox1-EGFP (43), female Pyy-EGFP mice (44), male and female Defa6-CreERT;Rosa26-tdTomato mice (45), and male and female Hopx-CreERT;Rosa26-tdTomato mice (JAX strains 017606, 007914). For the diet study, 8-10 week old C57BL/6 wild-type mice and, either 8-10 week old Lgr5-EGFP female mice (for histomorphometry and metabolic phenotyping) or adult 8–10 weeks old Sox9-EGFP female mice (for cell sorting and RNA sequencing), were fed *ad libitum* with either low-fat diet (LFD, 14% kcal from fat; Prolab RMH3000) or high-fat diet (HFD, 45% kcal from fat; Research Diets D12451) for 16 weeks. Body weight, body composition and blood parameters were measured to confirm obesity phenotype. To mark cells in S-phase, 5-ethynyl-2′deoxyuridine (EdU) was administered by ip injection (100 μg/25g body weight) 90 minutes prior to euthanizing. The harvested small intestine was divided into three equal segments. The middle region was considered jejunum. All animal procedures were performed with the approval and authorization of the Institutional Animal Care and Use Committee at each participating institution.

Flow cytometry. Six distinct reporter mouse strains that facilitate the sorting of a variety of different intestinal epithelial cell types were used to isolate aISCs (Lgr5-EGFP), EEC progenitors (Sox9-EGFP and Prox1-EGFP), mature EECs (Sox9-EGFP and Pyy-EGFP), Paneth cells (Defa6-CreERT2;Rosa26-tdTomato), and rISCs (Hopx-CreERT2;Rosa26-tdTomato). Mouse intestinal epithelial cells from the jejunum were dissociated and prepared for fluorescence-activated cell sorting (FACS) as described previously (20). CD31-APC (BioLegend, San Diego, CA), CD45-APC (BioLegend), and Annexin-V-APC (Life Technologies, Carlsbad, CA), and Sytox-Blue (Life Technologies) staining were used to exclude endothelial cells, immune cells, and apoptotic cells, respectively. The gating parameters of FACS sorting were described previously (20). The Lgr5, Sox9, and Defa6 sorts were performed using a Mo-Flo XDP cell sorter (Beckman-Coulter, Fullerton, CA) at the University of North Carolina Flow Cytometry Core Facility. The Prox1 sorts were performed using BD FACS Aria Fusion Fluorescence Activated Cell Sorter at Cornell University Flow Cytometry Core Facility at the Biotechnology Resource Center. The Pyy sorts were performed using BD FACSAria™ II Cell Sorter at Kings BRC flow cytometry Core facility. Sorting of Hopx+ cells was conducted at North Carolina State University, College of Veterinary Medicine using a Mo-Flo XDP cell sorter (Beckman-Coulter, Fullerton, CA). The cells were sorted directly into cold DMEM or lysis buffer.

Tuft cells were sorted by use of the cell surface marker Siglecf. Mouse jejnual cells were prepared as described previously (46). Aqua Live Dead fixable viability stain Live dye (ThermoFisher) and anti-mouse EpCam-APC (clone G8.8, ThermoFisher) staining was used to include viable, epithelial cells, respectively, while anti-mouse CD45 BV605 (clone 30-F11, BD

Biosciences) staining was used to exclude immune cells. Anti-mouse Siglecf-PE antibody (clone E50-2440, ThermoFisher) was employed to enrich for tuft cells. Sorting for tuft cells was performed using BD FACS Aria Fusion II Fluorescence Activated Cell Sorter (BD Biosciences) at Cornell University Flow Cytometry Core Facility, Biotechnology Resource Center. Cells were sorted directly into cold lysis buffer (Norgen).

Side population sorting was used to separate the sub-fraction of slowly cycling from active cycling intestinal stem cells, as described previously (18). Mouse intestinal epithelial cells from the jejunum of female C57BL/6 mice were prepared and sorted into either upper side population (consisting of actively cycling stem cells) or lower side population (consisting of slowly cycling stem cells) by the previously described gating methods (18). The side population sorting (46) was performed using a Mo-Flo XDP cell sorter (Beckman-Coulter, Fullerton, CA) at the University of North Carolina Flow Cytometry Core Facility. Cells were sorted directly into cold lysis buffer (Norgen).

Histological analysis. Mouse jejunal tissue was fixed in 4% (v/v) neutral-buffered paraformaldehyde, embedded in paraffin, and cut into 5μm sections for various staining experiments. Haemotoxylin and eosin (H&E) staining was performed for morphometric analyses (villi height and crypt density). Crypt density was calculated by dividing the number of well-oriented crypts per millimeter of submucosal circumference. EdU staining was performed to visualize cells in S-phase using the Click-iT EdU AlexaFluor 594 Kit (Invitrogen). Immunofluorescent staining of α-chromogranin (Chga) was performed for assessing mature EEC number. Briefly, sections were incubated with primary antibody (rabbit Chga, 1:100 dilution in

immunofluorescence buffer, Abcam ab15160) overnight at 4°C followed by Alexa flour 594 secondary antibody incubation for 2 hr at room temperature. DAPI (1:1000) was used to visualize nuclei. Images were captured using ZEISS Axiovert 200M inverted microscope. The numbers of Chga+ cells per villus were normalized by average villus height (mm) in each of the diet groups. For the villus height measurements, one data point from LFD group and one data point from HFD were removed as outliers after applying the criterion of value beyond average ± 1.5*standard deviation.

RNA extraction and real-time qPCR. Total RNA was isolated using the Total or Single-cell RNA Purification kit (Norgen Biotek, Thorold, ON, Canada). High Capacity RNA to cDNA kit (Life Technologies, Grand Island, NY) was used for reverse transcription of RNA. TaqMan microRNA Reverse Transcription kit (Life Technologies) was used for reverse transcription of miRNA. Both miRNA and gene expression qPCR were performed using TaqMan assays (Life Technologies) with either TaqMan Universal PCR Master Mix (miRNA qPCR) or TaqMan Gene Expression Master Mix (mRNA qPCR) per the manufacturer's protocol, on a BioRad CFX96 Touch Real Time PCR Detection System (Bio-Rad Laboratories, Richmond, CA). Reactions were performed in triplicate using either U6 (miRNA qPCR), Rps9 (mouse mRNA qPCR) or RNU48 (human mRNA qPCR) as the normalizer.

Small RNA library preparation and sequencing. The small RNA sequencing of cells from the various cell sorts and *D. melanogaster* midgut was conducted at Genome Sequencing Facility of Greehey Children's Cancer Research Institute at University of Texas Health Science Center at San Antonio. Libraries were prepared using the TriLink CleanTag Small RNA Ligation kit

(TriLink Biotechnologies, San Diego, CA). Seven to eight libraries were sequenced per lane, with single-end 50x on the HiSeq2500 platform. Raw sequencing data and miRNA quantification tables can be accessed through GEO record GSE118814.

RNA library preparation and sequencing. RNA-sequencing libraries from the Sox9 sorts of LFD-fed and HFD-fed C57BL/6J mice were prepared using the Clonetech SMARTer Ultra Low Input library preparation kit combined with Nextera XT DNA sample preparation kit (Illumina) and sequenced with single-end 100 bp on a HiSeq2000 platform at the UNC High Throughput Sequencing Core Facility, as previously described (47). Raw sequencing data as well as normalized counts are available through GEO accession GSE118814.

Single cell suspension preparation, RNA library preparation, and sequencing. Enteroids treated with either LNA7 or LNA-scramble were harvested at Day 5. Briefly, media was removed from enteroid cultures and the enteroids were washed twice with ice cold PBS. Enteroids were collected in cold PBS, spun down at 300xg for 5 minutes, and resuspended as a pellet in 10 mL of ice-cold D-PBS with 0.04% (w/v) BSA. Centrifugation at 1000xg at 4C was carried out for 5 minutes. Supernatant was removed and the pellet was resuspended in 10 mL of room temperature HBSS with 0.3 U/mL dispase. Incubation in a water bath was performed at 37°C for 12–16 minutes. The tubes were gently shaken every 2 minutes. An aliquot was examined under the microscope to determine whether >50% of the cells were single cells. Dispase activity was stopped by adding FBS to 10% of the total volume of samples and DNaseI to a final concentration of 50 μg/mL (50 μl). Samples were filtered with 40 μm strainer and centrifuged at 500xg at 4°C for 5 minutes. The supernatant was removed and the pellet was

resuspended in 10 mL of ice cold HBSS, and the samples were filtered again with 40 μm strainer and centrifuged at 500xg at 4°C for 5 minutes. The supernatant was removed and the pellet was resuspended in 100 μl of ice-cold D-PBS with 0.04% (w/v) BSA. The samples were gently mixed several times with wide-bore pipet tip (1000 μL pipet tip), and then checked under the microscope for any clumping. If clumps were present, the filtration, centrifugation, and resuspension steps were repeated. Finally, cell viability and cell number were determined using Trypan blue and BioRad cell counter in order to proceed with single cell library preparation and sequencing. For single cell sequencing, we used the 10X Genomics Chromium instrument at the Cornell Genomics Facility.

Bioinformatics analysis. *Bulk small RNA- and RNA-sequencing analysis* – Small RNA-sequencing reads were aligned to the mouse genome (mm9) and quantified using miRquant 2.0 as previously described (48), with the exception that raw miRNA counts were normalized using DESeq2 (49) to determine significance. Fruit fly sequences were depleted for a dominant rRNA species prior to alignment to the full genome (dm3). miRNA annotation was performed using miRbase (r18 for mouse and r21 for fruit fly). RNA-sequencing reads were mapped to mouse genome release mm10 using STAR (v2.5.3a) (50) and transcript quantification was performed using Salmon (v0.6.0) (51). Differential gene expression analysis was accomplished using DESeq2 (49).

Single cell RNA-sequencing analysis – Single cell RNA-sequencing reads for 107 LNA-7 and 158 LNA-scr cells were aligned to the mouse genome (mm10) and quantified using 10X Genomics CellRanger count. Cells with low gene complexity (<200 genes per cell) or with a

strong mitochondrial signature (>25% mitochondrial genes) were filtered, resulting in 92 LNA-7 and 140 LNA-scr cells. Cluster identification, differential expression analysis, and t-SNE plot generation were performed with Seurat_3.0.1.

Other – MiRNA binding site enrichment among differentially expressed genes was determined using miRhub (22). Transcription factor enrichment was determined by inputting the top 20 significant up-regulated genes into Enrichr (52, 53) and using the ENCODE and ChEA Consensus TFs from the ChIP-X dataset.

Enteroid culture. *Mouse enteroids* – Jejunal crypts were isolated from 3-5 months old female C57BL/6 mice as previously described (47). The isolated crypts (Day 0) were grown into Reduced Growth Factor Matrigel (cat. 356231, Corning). Advanced DMEM/F12 (cat. 12634-028, Gibco) supplemented with GlutaMAX (cat. 35050-061, Gibco), Pen/Strep (cat. 15140, Gibco), HEPES (cat. 15630-080, Gibco), N2 supplement (cat. 17502-048, Gibco), 50 ng/mL EGF (cat.2028-EG, R&D Systems), 100 µg/mL Noggin (cat. 250-38, PeproTech), 250 ng/µL murine R-spondin (cat. 3474-RS-050, R&D Systems), and 10 mM Y27632 (cat. ALX270-333-M025, Enzo Life Sciences) was added. For miRNA loss-of-function studies, miRCURY LNA Power Inhibitor against mouse miR-7 (mmu-miR-7a-5p) (cat. YI04100818-DDA, Qiagen) or Power Negative Control A (cat. YI00199006-DDA, Qiagen) was added at 500 nM on Day 0 and supplemented at 250 nM on Day 3. For miRNA gain-of-function studies, miRCURY LNA mimic of miR-7 (cat. YM00472714-AGA, Qiagen) or Negative Control (cat. YM00479902-AGA, Qiagen) was added at 500 nM on Day 0 and supplemented at 250 nM on Day 3. Enteroids

616 at Day 5 were harvested for RNA isolation or fixed in 2% (v/v) paraformaldehyde for whole
617 mount staining.
618
619 For studies knocking down *Egfr*, LNA-7 treated enteroids were treated with a custom LNA
620 GapmeR against Egfr (Egfr GapmeR-A Design ID: LG00204888-DDA, Egfr GapmeR-B Design
621 ID: LG00204889-DDA, Egfr GapmeR-C Design ID: LG00204890-DDA, Qiagen) or Negative
622 Control A Gapmer (Design ID: LG00000001-DDA, Qiagen) at 500 nM at Day 0 and
623 supplemented at 250 nM at Day 3. Enteroids at Day 5 were harvested for RNA isolation or fixed
624 in 2% (v/v) paraformaldehyde (PFA) for whole mount staining. For EdU staining assays,
625 enteroids were treated with 10 mM EdU 6 hr prior to the harvest time point follow by the
626 manufacturer's protocol of Click-iT™ EdU Alexa Fluor™ 488 Flow Cytometry Assay Kit
627 (C10425, ThermoFisher).
628
629 For studies inhibiting Xiap function, enteroids were treated with GDC0152 (SelleckChem; Cat. #
630 S7010), which inhibits the activity of IAPs (Inhibitors of Apoptosis Proteins) including X
631 chromosome-linked IAP (XIAP) and IAPs 1 and 2 and promote apoptosis. The enteroid culture
632 was treated alone with GDC0152 at 0.25 μm or co-treated with LNA at day 0. At day 5,
633 enteroids were fixed in 2% (v/v) paraformaldehyde for brightfield imaging and whole mount
634 staining.
635
636 *Porcine enteroids* – Jejunal crypts were isolated from 6–10 week-old, mixed gender, wild type
637 Yorkshire cross pigs as previously described (54). The isolated crypts (Day 0) were cultured in
638 Reduced Growth Factor Matrigel (cat. 356231, Corning) and maintained in DMEM/F12 medium

(cat. 12634-010, Life Technologies) supplemented with 50 ng/ml EGF (cat. 236-EG, R&D Systems), 100 ng/ml Noggin (cat. 120-10C, PeproTech), 1 µg/ml R-Spondin (cat. 4645RS/CF, R&D Systems), 500 nM A83-01 (cat. 2939, Tocris Bioscience), 10 µM SB202190 (cat. S7067, Sigma), 1 mM Nicotinamide (cat. N0636, Sigma), 10 nM Gastrin (cat. G9145, Sigma), 10 µM Y-27632 (cat. Y0503, Sigma) and 100 ng/ml Wnt3a (cat. 5036-WN/CF, R&D Systems). For miRNA studies, miRCURY LNA Power Inhibitor against miR-7 (mmu-miR-7a-5p miRCURY LNA miRNA Power Inhibitor, cat. YI04100818-DDA, Qiagen) or Power Negative Control A (cat. YI00199006-DDA, Qiagen) were added on Day 0 and enteroids were harvested on Day 3.

Human enteroids – Human duodenal enteroids were previously established from tissue collected from deceased donors through the Gift of Life, Michigan (University of Michigan IRB REP00000105; not regulated designation). For this study, specimen Duo-87 from a 21-year-old male were used (Translational Tissue Modeling Laboratory, TTML). Enteroids were cultured in medium containing 25% (v/v) L-WRN conditioned medium. The complete medium contained Advanced DMEM/F-12 (cat. 12634028, Gibco), 2 mM GlutaMax (cat. 35050-061, Gibco), 10 mM HEPES (cat. 15630080, Gibco), N-2 (cat. 17502048, Gibco), B-27 supplement minus vitamin A (cat. 12587010, Gibco), 50 units/mL penicillin, 0.05 mg/mL streptomycin (cat. 15070063, Gibco), 50 µg/ml Primocin (InvivoGen; ##ant-pm-1), 1 mM N-Acetyl-L-cysteine (Sigma-Aldrich, A9165), 50 ng EGF/mL (R&D Systems, Inc., 236-EG), 10 µM SB202190 (Sigma-Aldrich; S7067), 500 nM A83-01 (R&D Tocris, #2939), and 10 µM Y27632 (Tocris; 125410). Cultures were grown in Matrigel (diluted to 8mg/mL with growth media; Corning, #354234). Cultures were passaged by triturating and dissociating the Matrigel in cold DPBS, centrifuging at 300xg, and plating the first day with 2.5 µM CHIR99021 (Tocris; 4423). For

662 miRNA studies, miRCURY LNA Power Inhibitor against miR-7 (mmu-miR-7a-5p miRCURY
663 LNA miRNA Power Inhibitor Qiagen cat YI04100818-DDA) or Power Negative Control A
664 (Qiagen cat. YI00199006-DDA) were added on Day 0 and enteroids were harvested on Day 5.
665
666 ***Whole mount enteroids immunostaining and imaging.*** The fixed mouse enteroids were
667 permeabilized with 0.5% (v/v) Triton X-100/PBS, washed by PBS containing 0.1% (w/v)
668 BSA/0.02% (v/v) Triton-X/0.05% (v/v) Tween-20 and blocked with 10% (v/v) normal goat
669 serum. Primary antibodies were used to stain Chga (rabbit anti-Chga, 1:100, Abcam ab15160)
670 and PH3 (rabbit anti- Phospho-Histone H3 (Ser10), 1:100, Cell Signaling 9701S) and Xiap
671 (1:100; rabbit, Novus Biologicals NBP2-20918). The staining was visualized by fluorescence
672 microscopy with fluorescent-conjugated secondary antibodies (goat anti rabbit Alexa Fluor 488,
673 1:400, ThermoFisher, Cat. # A-11034). Nuclei were counterstained with Hoechst 33258 dye
674 (1:1000). For EdU staining assays, enteroids were treated with 10 mM EdU 6 hr prior to the
675 harvest time point follow by the manufacturer's protocol of Click-iT™ Plus EdU Alexa Fluor™
676 488/594 imaging Kit (C10637, C10639 ThermoFisher Scientific). The immunofluorescent
677 staining was visualized by ZEISS Axiovert 200M inverted microscope. The z-stack bright field
678 images were taken by ZEISS Axiovert 200M inverted microscope for bud count analysis.
679
680 ***Ecc15 infection in Drosophila melanogaster.*** Wide type line Canton-S (BDSC: 64349) was
681 maintained at room temperature (~23˚C) on standard fly medium (50 g baker yeast, 30 g
682 cornmeal, 20 g sucrose,15 g agar, 5 mL 99% (v/v) propionic acid mix, 0.5 mL 85% (v/v)
683 phosphoric acid, 26.5 mL methyl paraben in ethanol per 1 L) in a 12:12 hours light/dark cycle.
684 Oral infection of pathogen *Erwinia carotovora ssp. carotovora* 15 (*Ecc*15) was performed as

previously described (25). Orally treated flies were incubated at 29˚C until dissection for analyses.

Generation of genetically modified lines of Drosophila. Esg-Gal4; UAS-GFP, tub-Gal80^{TS} (Esg^{TS}, progenitor specific) (55) and Uas lines (BDSC 41137) were used for creating flies with miR-7 overexpression in Esg stem/progenitor cells. Genetic crosses for flies containing Gal4-UAS-Gal80 system were crossed using ~15 female flies and 5 males, and transferred during development in a 12:12 hour light/dark 18˚C incubator. Parental generation was removed after 5 days in the 18˚C incubator to control for fly density of the F1 progeny.

Immunostaining of Drosophila midgut. The excised Drosophila midguts were fixed in 4% paraformaldehyde and washed with 0.1% (w/v) Triton X-100 in PBS. The samples then incubated for an hour in blocking solution (1% (w/v) BSA, 1% (v/v) normal donkey serum, and 0.1% (w/v) Triton X-100 in PBS) followed by overnight primary antibody incubation and 2 hours secondary antibody staining. Primary antibodies used in this study were rabbit anti-PH3 (1:000, EMD Millipore). Secondary antibodies used in this study were donkey anti-rabbit-555 (1:2000, Thermo Fisher). DAPI (1:50000) was used to visualize nuclei. Imaging was performed on a Zeiss LSM 700 fluorescent/ confocal inverted microscope. PH3 positive cells were manually counted along the surface of the midgut.

Statistics. In most figure panels, quantitative data are reported as an average of biological replicates ± standard error of the mean. In figure panels pertaining to bright field bud count analysis and whole mount immunofluorescent staining in enteroids, quantitative data are reported as an average of values from all the enteroids pooled from multiple independent experiments ± standard error of the mean (n=2-7 wells per condition per experiment). In all analyses, statistical

differences were assessed by two-tailed Student's t-test with threshold P-value < 0.05, unless otherwise specifically noted.

All authors had access to the study data and had reviewed and approved the final manuscript.

References

1. Clevers H. The intestinal crypt, a prototype stem cell compartment. Cell. 2013;154(2):274-84.
2. Smith NR, Gallagher AC, Wong MH. Defining a stem cell hierarchy in the intestine: markers, caveats and controversies. The Journal of physiology. 2016;594(17):4781-90.
3. Jadhav U, Saxena M, O'Neill NK, Saadatpour A, Yuan GC, Herbert Z, et al. Dynamic Reorganization of Chromatin Accessibility Signatures during Dedifferentiation of Secretory Precursors into Lgr5+ Intestinal Stem Cells. Cell Stem Cell. 2017;21(1):65-77 e5.
4. Yan KS, Gevaert O, Zheng GXY, Anchang B, Probert CS, Larkin KA, et al. Intestinal Enteroendocrine Lineage Cells Possess Homeostatic and Injury-Inducible Stem Cell Activity. Cell Stem Cell. 2017;21(1):78-90 e6.
5. Ivey KN, Srivastava D. MicroRNAs as regulators of differentiation and cell fate decisions. Cell Stem Cell. 2010;7(1):36-41.
6. Peng Y, Croce CM. The role of MicroRNAs in human cancer. Signal Transduct Target Ther. 2016;1:15004.
7. Hung YH, Sethupathy P. MicroRNAs in the Mammalian Gut Endocrine Lineage. Endocrinology. 2018;159(2):866-8.
8. Latreille M, Hausser J, Stutzer I, Zhang Q, Hastoy B, Gargani S, et al. MicroRNA-7a regulates pancreatic beta cell function. J Clin Invest. 2014;124(6):2722-35.
9. Poy MN. MicroRNAs: An adaptive mechanism in the pancreatic beta-cell...and beyond? Best Pract Res Clin Endocrinol Metab. 2016;30(5):621-8.
10. Lopez-Beas J, Capilla-Gonzalez V, Aguilera Y, Mellado N, Lachaud CC, Martin F, et al. miR-7 Modulates hESC Differentiation into Insulin-Producing Beta-like Cells and Contributes to Cell Maturation. Mol Ther Nucleic Acids. 2018;12:463-77.
11. Xu H, Guo S, Li W, Yu P. The circular RNA Cdr1as, via miR-7 and its targets, regulates insulin transcription and secretion in islet cells. Sci Rep. 2015;5:12453.
12. Wang Y, Liu J, Liu C, Naji A, Stoffers DA. MicroRNA-7 regulates the mTOR pathway and proliferation in adult pancreatic beta-cells. Diabetes. 2013;62(3):887-95.
13. Bravo-Egana V, Rosero S, Molano RD, Pileggi A, Ricordi C, Dominguez-Bendala J, et al. Quantitative differential expression analysis reveals miR-7 as major islet microRNA. Biochem Biophys Res Commun. 2008;366(4):922-6.
14. Kredo-Russo S, Mandelbaum AD, Ness A, Alon I, Lennox KA, Behlke MA, et al. Pancreas-enriched miRNA refines endocrine cell differentiation. Development. 2012;139(16):3021-31.
15. Downing S, Zhang F, Chen Z, Tzanakakis ES. MicroRNA-7 directly targets Reg1 in pancreatic cells. Am J Physiol Cell Physiol. 2019;317(2):C366-C74.
16. Knudsen LA, Petersen N, Schwartz TW, Egerod KL. The MicroRNA Repertoire in Enteroendocrine Cells: Identification of miR-375 as a Potential Regulator of the Enteroendocrine Lineage. Endocrinology. 2015;156(11):3971-83.
17. Heverhagen AE, Legrand N, Wagner V, Fendrich V, Bartsch DK, Slater EP. Overexpression of MicroRNA miR-7-5p Is a Potential Biomarker in Neuroendocrine Neoplasms of the Small Intestine. Neuroendocrinology. 2018;106(4):312-7.

18. von Furstenberg RJ, Buczacki SJ, Smith BJ, Seiler KM, Winton DJ, Henning SJ. Side population sorting separates subfractions of cycling and non-cycling intestinal stem cells. Stem Cell Res. 2014;12(2):364-75.
19. Richards P, Pais R, Habib AM, Brighton CA, Yeo GS, Reimann F, et al. High fat diet impairs the function of glucagon-like peptide-1 producing L-cells. Peptides. 2016;77:21-7.
20. Mah AT, Van Landeghem L, Gavin HE, Magness ST, Lund PK. Impact of diet-induced obesity on intestinal stem cells: hyperproliferation but impaired intrinsic function that requires insulin/IGF1. Endocrinology. 2014;155(9):3302-14.
21. Beyaz S, Mana MD, Roper J, Kedrin D, Saadatpour A, Hong SJ, et al. High-fat diet enhances stemness and tumorigenicity of intestinal progenitors. Nature. 2016;531(7592):53-8.
22. Baran-Gale J, Fannin EE, Kurtz CL, Sethupathy P. Beta cell 5'-shifted isomiRs are candidate regulatory hubs in type 2 diabetes. PLoS One. 2013;8(9):e73240.
23. Liu S, Zhang P, Chen Z, Liu M, Li X, Tang H. MicroRNA-7 downregulates XIAP expression to suppress cell growth and promote apoptosis in cervical cancer cells. FEBS Lett. 2013;587(14):2247-53.
24. Sato T, Vries RG, Snippert HJ, van de Wetering M, Barker N, Stange DE, et al. Single Lgr5 stem cells build crypt-villus structures in vitro without a mesenchymal niche. Nature. 2009;459(7244):262-5.
25. Buchon N, Broderick NA, Poidevin M, Pradervand S, Lemaitre B. Drosophila intestinal response to bacterial infection: activation of host defense and stem cell proliferation. Cell Host Microbe. 2009;5(2):200-11.
26. Tsai YH, Czerwinski M, Wu A, Dame MK, Attili D, Hill E, et al. A Method for Cryogenic Preservation of Human Biopsy Specimens and Subsequent Organoid Culture. Cell Mol Gastroenterol Hepatol. 2018;6(2):218-22 e7.
27. Huang C, Zeng X, Jiang G, Liao X, Liu C, Li J, et al. XIAP BIR domain suppresses miR-200a expression and subsequently promotes EGFR protein translation and anchorage-independent growth of bladder cancer cell. J Hematol Oncol. 2017;10(1):6.
28. Basak O, Beumer J, Wiebrands K, Seno H, van Oudenaarden A, Clevers H. Induced Quiescence of Lgr5+ Stem Cells in Intestinal Organoids Enables Differentiation of Hormone-Producing Enteroendocrine Cells. Cell Stem Cell. 2017;20(2):177-90 e4.
29. Liu X, Li G, Su Z, Jiang Z, Chen L, Wang J, et al. Poly(amido amine) is an ideal carrier of miR-7 for enhancing gene silencing effects on the EGFR pathway in U251 glioma cells. Oncol Rep. 2013;29(4):1387-94.
30. Sun X, Li J, Sun Y, Zhang Y, Dong L, Shen C, et al. miR-7 reverses the resistance to BRAFi in melanoma by targeting EGFR/IGF-1R/CRAF and inhibiting the MAPK and PI3K/AKT signaling pathways. Oncotarget. 2016;7(33):53558-70.
31. Trajkovski M, Hausser J, Soutschek J, Bhat B, Akin A, Zavolan M, et al. MicroRNAs 103 and 107 regulate insulin sensitivity. Nature. 2011;474(7353):649-53.
32. Poy MN, Hausser J, Trajkovski M, Braun M, Collins S, Rorsman P, et al. miR-375 maintains normal pancreatic alpha- and beta-cell mass. Proc Natl Acad Sci U S A. 2009;106(14):5813-8.
33. Soh J, Iqbal J, Queiroz J, Fernandez-Hernando C, Hussain MM. MicroRNA-30c reduces hyperlipidemia and atherosclerosis in mice by decreasing lipid synthesis and lipoprotein secretion. Nat Med. 2013;19(7):892-900.
34. Li X, Cassidy JJ, Reinke CA, Fischboeck S, Carthew RW. A microRNA imparts robustness against environmental fluctuation during development. Cell. 2009;137(2):273-82.
35. Gunawardene AR, Corfe BM, Staton CA. Classification and functions of enteroendocrine cells of the lower gastrointestinal tract. Int J Exp Pathol. 2011;92(4):219-31.
36. Beumer J, Artegiani B, Post Y, Reimann F, Gribble F, Nguyen TN, et al. Enteroendocrine cells switch hormone expression along the crypt-to-villus BMP signalling gradient. Nature cell biology. 2018;20(8):909-16.
37. Shivdasani RA. Limited gut cell repertoire for multiple hormones. Nature cell biology. 2018;20(8):865-7.

802 38. Hutch CR, Sandoval D. The Role of GLP-1 in the Metabolic Success of Bariatric Surgery.
803 Endocrinology. 2017;158(12):4139-51.
804 39. Worthington JJ. The intestinal immunoendocrine axis: novel cross-talk between enteroendocrine
805 cells and the immune system during infection and inflammatory disease. Biochem Soc Trans.
806 2015;43(4):727-33.
807 40. Moran GW, Leslie FC, Levison SE, Worthington J, McLaughlin JT. Enteroendocrine cells:
808 neglected players in gastrointestinal disorders? Therap Adv Gastroenterol. 2008;1(1):51-60.
809 41. Zietek T, Rath E. Inflammation Meets Metabolic Disease: Gut Feeling Mediated by GLP-1. Front
810 Immunol. 2016;7:154.
811 42. Formeister EJ, Sionas AL, Lorance DK, Barkley CL, Lee GH, Magness ST. Distinct SOX9 levels
812 differentially mark stem/progenitor populations and enteroendocrine cells of the small intestine
813 epithelium. Am J Physiol Gastrointest Liver Physiol. 2009;296(5):G1108-18.
814 43. Choi I, Chung HK, Ramu S, Lee HN, Kim KE, Lee S, et al. Visualization of lymphatic vessels by
815 Prox1-promoter directed GFP reporter in a bacterial artificial chromosome-based transgenic mouse.
816 Blood. 2011;117(1):362-5.
817 44. Bohorquez DV, Chandra R, Samsa LA, Vigna SR, Liddle RA. Characterization of basal
818 pseudopod-like processes in ileal and colonic PYY cells. Journal of molecular histology. 2011;42(1):3-13.
819 45. King SL, Mohiuddin JJ, Dekaney CM. Paneth cells expand from newly created and preexisting
820 cells during repair after doxorubicin-induced damage. Am J Physiol Gastrointest Liver Physiol.
821 2013;305(2):G151-62.
822 46. Gerbe F, Sidot E, Smyth DJ, Ohmoto M, Matsumoto I, Dardalhon V, et al. Intestinal epithelial
823 tuft cells initiate type 2 mucosal immunity to helminth parasites. Nature. 2016;529(7585):226-30.
824 47. Peck BC, Mah AT, Pitman WA, Ding S, Lund PK, Sethupathy P. Functional Transcriptomics in
825 Diverse Intestinal Epithelial Cell Types Reveals Robust MicroRNA Sensitivity in Intestinal Stem Cells to
826 Microbial Status. J Biol Chem. 2017;292(7):2586-600.
827 48. Kanke M, Baran-Gale J, Villanueva J, Sethupathy P. miRquant 2.0: an Expanded Tool for
828 Accurate Annotation and Quantification of MicroRNAs and their isomiRs from Small RNA-Sequencing
829 Data. J Integr Bioinform. 2016;13(5):307.
830 49. Love MI, Huber W, Anders S. Moderated estimation of fold change and dispersion for RNA-seq
831 data with DESeq2. Genome Biol. 2014;15(12):550.
832 50. Dobin A, Davis CA, Schlesinger F, Drenkow J, Zaleski C, Jha S, et al. STAR: ultrafast universal
833 RNA-seq aligner. Bioinformatics. 2013;29(1):15-21.
834 51. Patro R, Duggal G, Love MI, Irizarry RA, Kingsford C. Salmon provides fast and bias-aware
835 quantification of transcript expression. Nat Methods. 2017;14(4):417-9.
836 52. Chen EY, Tan CM, Kou Y, Duan Q, Wang Z, Meirelles GV, et al. Enrichr: interactive and
837 collaborative HTML5 gene list enrichment analysis tool. BMC Bioinformatics. 2013;14:128.
838 53. Kuleshov MV, Jones MR, Rouillard AD, Fernandez NF, Duan Q, Wang Z, et al. Enrichr: a
839 comprehensive gene set enrichment analysis web server 2016 update. Nucleic Acids Res.
840 2016;44(W1):W90-7.
841 54. Gonzalez LM, Williamson I, Piedrahita JA, Blikslager AT, Magness ST. Cell lineage
842 identification and stem cell culture in a porcine model for the study of intestinal epithelial regeneration.
843 PLoS One. 2013;8(6):e66465.
844 55. Micchelli CA, Perrimon N. Evidence that stem cells reside in the adult Drosophila midgut
845 epithelium. Nature. 2006;439(7075):475-9.

846

847

Figure legends.

Figure 1. MicroRNA-7 is highly enriched in the enteroendocrine (EEC) lineage trajectory. **a**, Schematic diagram of different sorted cell populations representing specific cell lineages in the small intestine. **b**, Level of expression (RNA-seq) of specific marker genes in each of the Sox9-Low (n=4), Sox9-High (n=3), and Sox9-Negative (n=4) populations of cells. **c**, Hierarchical clustering analysis based on the expression profiles of the top 50 most variable miRNAs across the different sorted cell populations shown in the heat map (Sox9-Low, n=3; Sox9-High, n=3; Sox9-Negative, n=3; Sox9-Sublow, n=3; Sox9-Unsorted, n=2; Lgr5-High, n=2; Hopx+, n=4; Prox1+, n=3). **d**, MiR-7a/b expression in the EEC lineage vs. non-EEC absorptive lineage. Similar data for miR-194 and miR-215 provided for sake of comparison. **e**, RT-qPCR data showing enrichment of *Hopx* and miR-7 in Hopx+ cells (n=4) relative to Hopx- cells (n=4). **f**, RT-qPCR data showing enrichment of miR-7, *Lgr5*, and *Chga* in lower side population (LSP, n=2) relative to upper side population (USP, n=2) and Lgr5+ cells (n=2). **g**, RT-qPCR data showing enrichment of *Prox1*, miR-7, and *Chga* in Prox1+ cells (n=3) compared with Prox1- cells (n=3). **h**, Scatter plot showing abundance (y-axis) and enrichment (x-axis) of all detected miRNAs in Prox1+ cells (n=3) relative to Prox1- cells (n=3). MiRNAs above expression of 1000 reads per million mapped to miRNAs (RPMMM) and 5-fold enrichment are shown in red (n=10). Among these, miR-7b is highlighted in blue. **i**, Fold-difference in expression of the 10 miRNAs highlighted in panel (f) in Prox1+ cells (n=3) relative to Lgr5+ cells (n=2) highlights miR-7 (blue) as a robust EEC progenitor cell enriched miRNA. **j**, Left: RT-qPCR data showing enrichment of *Lyz1* (marker of Paneth cells) in Defa6+ (n=4) relative to Defa6- cells (n=4). Middle: RT-qPCR data showing enrichment of Dclk1 (marker of tuft cells) in Siglecf+/CD45-/EpCam+ cells (n=2) relative to unsorted cells (n=2). Right: RT-qPCR data showing miR-7

871 enrichment in EECs (Sox9-High; n=3) compared to Paneth and tuft cells. * P < 0.05, ** P <
872 0.01, *** P < 0.001 by two-tailed Student's t-test. RQV, relative quantitative value.
873
874 **Figure 2. MiR-7 expression is suppressed and predicted miR-7 targets are elevated in EEC**
875 **progenitors under conditions of increased intestinal crypt division and reduced EEC**
876 **abundance. A**, Representative H&E images and crypt density quantification of mid-jejunum
877 from HFD-fed (n=9) and LFD-fed (n=8) mix of Lgr5-EGFP reporter mice and naïve C57BL/6
878 WT mice. Bar = 100 µm. **B**, Representative images of tissue sections stained with Hoechst
879 (blue) and EdU (red) and quantification of EdU+ cells per crypt from HFD-fed (n=8) and LFD-
880 fed (n=7) Lgr5-EGFP reporter mice and naïve C57BL/6 WT mice. **C**, Representative images of
881 tissue sections stained with Chga and quantification of Chga+ cells per villi (normalized by villi
882 height) from HFD-fed (n=7) and LFD-fed (n=4) mix of Lgr5-EGFP reporter mice and C57BL/6
883 naïve WT mice. **D,** Schematic of experimental workflow using Sox9-EGFP reporter mice. **E**,
884 PCA plot of small RNA-seq data of Sox9-Low cells from HFD-fed and LFD-fed Sox9-EGFP
885 reporter mice. **F**, Volcano plot of differentially expressed miRNAs in HFD-fed relative to LFD-
886 fed Sox9-EGFP reporter mice (dashed lines represent fold-change > 2). **G**, miRNAs that are
887 significantly (P < 0.05) upregulated or downregulated in jejunal Sox9-Low sorted cells from
888 HFD-fed relative to LFD-fed mice. Red and blue bars highlight miRNAs with greater than 2-
889 fold change up or down, respectively, in HFD-fed relative to LFD-fed mice. **H**, Expression level
890 of miR-7b (small RNA-seq) in Sox9-Low and Sox9-High cells from HFD-fed and LFD-fed
891 Sox9-EGFP mice. **I**, PCA plot of RNA-seq data of Sox9-Low cells from HFD-fed and LFD-fed
892 mice. **J**, Volcano plot of differentially expressed genes in HFD-fed relative to LFD-fed Sox9-
893 EGFP reporter mice (dashed line represents adjusted P < 0.05). **K**, Heatmap showing changes in

894 genes involved in proliferation, EEC differentiation, and enterocyte differentiation of jejunal
895 Sox9-Low cells of HFD-fed relative to LFD-fed mice. **L**, Enrichment analysis of miRNA target
896 sites (using the Monte Carlo simulation tool miRhub) in genes upregulated in response to HFD
897 (dashed line represents $P < 0.05$). Only miRNAs down-regulated greater than 2-fold in Sox9-
898 Low cells from HFD-fed relative to LFD-fed mice are included in the analysis. **M**, Sequencing
899 data showing upregulation of miR-7 target gene *Xiap* in Sox9-Low cells from HFD-fed relative
900 to LFD-fed mice. **N**, Inverse correlation between expression level of miR-7b and *Xiap* among the
901 HFD-fed and LFD-fed Sox9-EGFP reporter mice. All figure panels from (e) onward correspond
902 to data from n=4 HFD-fed and n=4 LFD-fed Sox9-EGFP reporter mice. * $P < 0.05$, ** $P < 0.01$
903 by two-tailed Student's t-test.
904
905 **Figure 3. MiR-7 controls intestinal epithelial growth *ex vivo*. A,** Experimental design for
906 testing the effect of miR-7 suppression in enteroid culture established from C57BL/6 WT mouse
907 jejunum. **B,** RT-qPCR data showing effective suppression of miR-7 expression by locked
908 nucleic acid (LNA-7) treatments in mouse enteroids compared with mock (no treatment) and
909 LNA-scramble (LNA-scr) control (n=5-6 wells per condition pooled from two independent
910 experiments). **C**, Small RNA-seq followed by differential expression analysis showing highly
911 robust and specific suppression of all the miR-7 family members in the enteroids treated with
912 LNA-7 compared to LNA-scr (LNA-7, n=6; LNA-scr, n=5). **D**, Representative bright field
913 images of enteroids treated with mock, LNA-scr, and LNA-7. **E,** Bar graph depicting average
914 number of buds / enteroid in the indicated treatment groups**.** Data were pooled from 3
915 independent experiments (mock, n=174; LNA-scr, n=214; LNA-7, n=163 enteroids). **F**, Left:
916 RT-qPCR data showing effective suppression of miR-7 by LNA-7 (n=5 wells/condition) in

porcine enteroids. Right: bar graph depicting average number of buds / porcine enteroid in the indicated treatment groups. Enteroids were pooled from 5 independent experiments (Mock, n=83; LNA-7, n=86 enteroids). **G**, Representative images of mouse enteroids showing whole mount staining signal for EdU (green; top) and PH3 (red; bottom). **H**, Bar graph depicting average number of PH3+ cells per enteroid. All of the enteroids across multiple wells were examined (mock, n=100; LNA-scr, n=83; LNA-7, n=106 enteroids). **I**, RT-qPCR data showing effective increase in miR-7 levels in mouse enteroids treated with mimics of miR-7 (mimics-miR-7) compared with mock (no treatment) and mimics-scramble (mimics-scr) (n=3 wells per group). **J**, Representative brightfield images of WT mouse enteroids (top) and whole mount staining signal for PH3 (red) (bottom) in the indicated treatments. **K**, Quantification of the average number of buds per enteroid in the indicated treatments. Enteroids per treatment group were pooled from multiple wells for quantification (Mock, n=175; mimics-scr, n=168; mimics-miR-7, n=116). **L**, Quantification of the average number of PH3+ cells per enteroid in the indicated treatments. All of the enteroids across multiple wells were examined (mock, n=123; mimics-scr, n=190; mimics-miR-7, n=165 enteroids). * $P < 0.05$, ** $P < 0.01$ and *** $P < 0.001$ by two-tailed Student's t test. RQV, relative quantitative value.

Figure 4. MiR-7 controls intestinal epithelial proliferation in *Drosophila* midgut *in vivo*. A, Mature miR-7 sequence across different species, including human, pig, mouse and fruit fly. The seed sequence is denoted in red. **B**, Heatmap results of small RNA-seq analysis of *D. melanogaster* midgut showing miRNAs that are significantly ($P < 0.05$) upregulated or downregulated upon exposure to the pro-proliferative *Ecc*15 pathogen (n=3) relative to unchallenged (UC) condition (n=3). Only showing those miRNAs with average reads per

940 million mapped to miRNAs (RPMMM) > 100 in either *Ecc*15 challenge or UC. **C**,
941 Downregulation of miR-7 in the *D. melanogaster* midgut at 4 hours (minimal proliferative
942 response, n=3) and 12 hours (peak proliferative response, n=3) after *Ecc*15 challenge compared
943 to the UC control group. **D**, Immunofluorescent staining of DAPI (blue) and Esg (green) in *D.*
944 *melanogaster* midgut with mock (left), Ecc15 alone (middle), and Ecc15 with miR-7
945 overexpression driven by the Esg promoter (miR-7 OE) (right). **E**, Bar graph showing counts of
946 PH3+ replicating cells in the *D. melanogaster* midgut of each. * $P < 0.05$, ** $P < 0.01$ and *** P
947 < 0.001 by two-tailed Student's t-test.
948
949 **Figure 5. MiR-7 control of enteroid budding is dependent on intact Xiap. A**, t-SNE plot of
950 single cell RNA-seq profiles reveals three major cell populations: enterocytes, Paneth cells, and
951 progenitor/stem cells, from mouse enteroids treated with LNA-7 or LNA-scr (enterocytes, n=107
952 cells; Paneth cells, n=54; progenitor/stem, n=71). The clusters were assigned based on overlap
953 with marker genes for every major intestinal epithelial cell type defined in Haber et al., 2017. **B**,
954 t-SNE plot of single cell RNA-seq data showing expression level for *Apoa1* (top, enterocyte
955 marker) and *Cenpa* (bottom, progenitor cell marker). **C,** Heat map displaying average
956 expression of cell type-specific markers for cells in each cluster from LNA-scr and LNA-7
957 treated mouse enteroids. Expression is scaled by row. **D,** Average *Xiap* expression across all
958 cells from LNA-scr or LNA-7 treated mouse enteroids (Wilcox). **E**, Percentage of *Xiap*+ cells
959 present in the scRNA-seq data from mouse enteroids treated with LNA-scr or LNA-7. **F,**
960 Percentage of Xiap+ progenitor/stem cells present in the scRNA-seq data from mouse enteroids
961 treated with LNA-scr or LNA-7. **G**, RT-qPCR data showing suppression of miR-7 (left panel)
962 and the upregulation of *XIAP* (right panel) in human intestinal organoids (HIOs) treated with

963 LNA-7 compared to LNA-scr (n=3 wells per condition). RQV, relative quantitative value. **H**,
964 Representative images and quantification of whole mount staining signal for Xiap (red) and
965 Hoechst (blue) in mouse enteroids with the indicated treatment groups (mock, n= 99; GDC0152,
966 n= 69 enteroids). **I**, Representative bright field images and quantification of average number of
967 buds per enteroid with mock treatment (no treatment) or Xiap inhibitor treatment (GDC0152)
968 (mock, n=274; GDC0152, n=120 enteroids). **J**, Representative images and quantification of
969 whole mount staining signal for Xiap (red) and Hoechst (blue) in the indicated treatment groups.
970 Data from enteroids across multiple wells were examined (LNA-scr, n=112 enteroids; LNA-7,
971 n=41; GDC0152+LNA-scr, n= 18; GDC0152+LNA-7 = 32). **K**, Representative bright field
972 images and quantification of the average number of buds per enteroid after LNA-scr treatment or
973 LNA-7 treatment with and without GDC0152 (LNA-scr, n=192 enteroids; LNA-7, n=118;
974 GDC0152+LNA-scr, n=96; GDC0152+LNA-7, n = 44). **L**, Representative images and
975 quantification of whole mount staining signal for PH3 (red) and Hoechst (blue) in the indicated
976 treatment groups. Data from enteroids across multiple wells were examined (LNA-scr, n=92
977 enteroids; LNA-7, n=45; GDC0152+LNA-scr, n= 58; GDC0152+LNA-7 = 62). * $P < 0.05$, ** $P < 0.01$ and *** $P < 0.001$ by two-tailed Student's t-test.
978
979
980 **Figure 6. MiR-7 control of enteroid budding depends on Egfr signaling.** **A**, RT-qPCR data
981 showing *Egfr* expression in mouse enteroids treated with control Gapmer inhibitor (n=2) or Egfr
982 Gapmer inhibitor (n=2) on Day 5. **B,** Quantification of the average number of buds per enteroid
983 treated with mock (no treatment), Gapmer Control, or Gapmer Egfr (Mock, n=194; Gapmer
984 Control, n=88; Gapmer Egfr, n = 149 enteroids). **C**, Representative bright field images of mouse
985 enteroids with treatment of Gapmer Control and Gapmer Egfr. **D,** Quantification of the average

number of buds per mouse enteroid in the indicated treatments (LNA-7, n=55; LNA-7 + Gapmer control, n=53; LNA-7 + Egfr Gapmer, n=27 enteroids). **E**, Representative images showing whole mount staining of EdU (top; red), Hoechst (top; blue), and bright field (bottom) in mouse enteroids with the indicated treatments. **F**, Quantification of the average number of buds per mouse enteroid in the indicated treatments (LNA-scr, n=165; LNA-7, n=182; LNA-scr + Gapmer Egfr, n=91; LNA-7 + Gapmer Egfr, n=148 enteroids). **G**, Percentage of *Prox1*+ progenitor/stem cells present in the scRNA-seq data from mouse enteroids treated with LNA-scr or LNA-7. **H,** Percentage of *Chga*+ progenitor/stem cells present in the scRNA-seq data from mouse enteroids treated with LNA-scr or LNA-7. **I**, Representative images of Prox1+ cells (green) and quantification of Prox1+ cells per mouse enteroid established from Prox1-EGFP reporter mice in the indicated treatments (mock, n=30; LNA-scr, n=46; LNA-7, n=26 enteroids). **J**, Representative images of Chga+ cells (red) and quantification of Chga+ cells per mouse enteroid in the indicated treatments (mock, n=96; LNA-scr, n=92; LNA-7, n=113 enteroids pooled from two independent experiments). **K**, The proposed partial working model of miR-7 control of intestinal epithelial proliferation. * $P < 0.05$, ** $P < 0.01$ and *** $P < 0.001$ by two-tailed Student's t-test.

Table 1. Small RNA-seq profiling followed by enrichment analysis of miRNAs in stem/EEC progenitors (Sox9-Low, n=3) and in mature EECs (Sox9-High, n=3) relative to unsorted intestinal epithelial cells (n=2). Only miRNAs that have an average reads per million mapped to miRNAs (RPMMM) > 100 in either Sox9-Low or Sox9-High and have less than a 2-fold enrichment in Sox9-Sublow (transit-amplifying cells) and Sox9-Negative (enterocytes) are shown.

Class A **miRNAs enriched in mature EEC (Sox9-High)**	**Class B** **miRNAs enriched in progenitor EEC (Sox9-Low)**	**Class C** **miRNAs enriched in both mature and progenitor EECs**
miR-139-3p	miR-181c-3p	let-7e-5p
miR-182-5p	miR-181d-5p	miR-1224-5p
miR-182-5p_+_1		miR-125a-5p
miR-183-5p		miR-132-3p
miR-183-5p_+_1		miR-184-3p
miR-328-3p		miR-375-3p
miR-672-5p		miR-375-3p_-_1
miR-744-5p		miR-375-3p_+_1
		miR-375-3p_+_2
		miR-7a-2-3p
		miR-7b-5p
		miR-7b-5p_+_1
		miR-92b-3p
		miR-99b-5p

Table 2. Small RNA-seq analysis showing differentially expressed miRNAs (adjusted P < 0.05) in mouse enteroids treated with LNA-7 (n = 6) relative to LNA-scr (n = 5).

miRNA	**log2FoldChange**	**p-adjusted**
mmu-mir-7a-1-5p	-7.109435038	4.64E-43
mmu-mir-7a-2-5p	-7.103216777	5.31E-43
mmu-let-7f-1-5p	-0.854266518	8.57E-14
mmu-let-7f-2-5p	-0.862650621	1.58E-13
mmu-mir-215-5p	-1.460451901	3.96E-10
mmu-mir-148a-3p	0.495197848	5.41E-05
mmu-mir-215-5p_+_1	-1.050094118	1.02E-04
mmu-mir-192-5p_+_2	0.309404578	2.82E-04
mmu-mir-98-5p	-0.509809453	4.18E-04
mmu-let-7i-5p	-0.402567428	0.001535664
mmu-mir-30d-5p	0.317770352	0.004397959
mmu-mir-26a-2-5p	0.149129242	0.004685784
mmu-mir-26a-1-5p	0.149100629	0.004685784
mmu-mir-203-3p_+_1	0.592648674	0.009726977
mmu-mir-30e-3p	0.276607739	0.010577384
mmu-mir-192-5p_+_1	0.204704048	0.010887894
mmu-mir-192-5p	0.206058351	0.01488005
mmu-let-7g-5p	-0.48204363	0.035030773

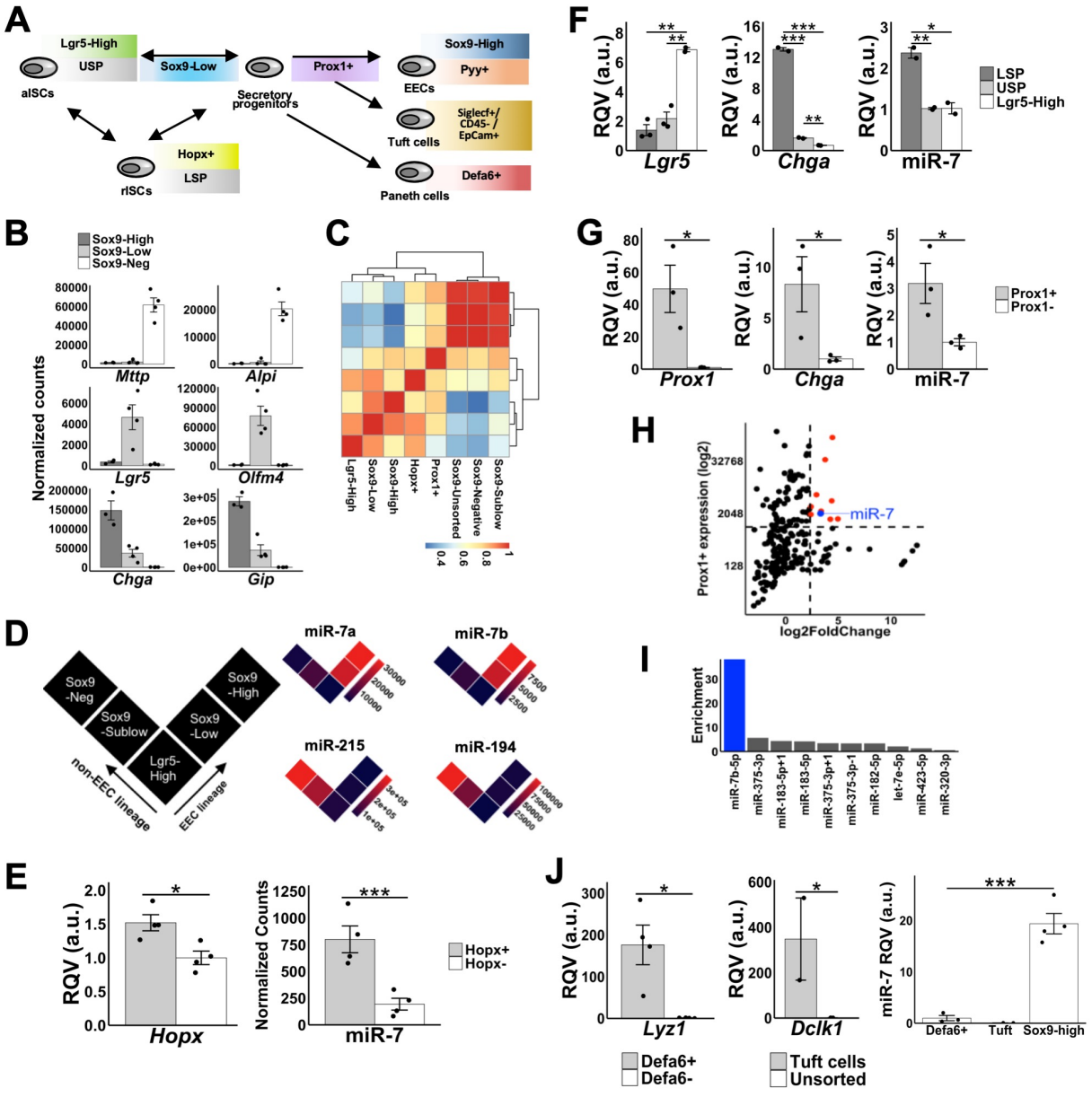
A
Lgr5-High
USP
Sox9-Low
Prox1+
Sox9-High
Pyy+
aISCs
Secretory progenitors
EECs
Siglecf+/ CD45- / EpCam+
Tuft cells
Hopx+
LSP
rISCs
Defa6+
Paneth cells
B
Sox9-High
Sox9-Low
Sox9-Neg
Normalized counts
Mttp
Alpi
Lgr5
Olfm4
Chga
Gip
C
Lgr5-High
Sox9-Low
Sox9-High
Hopx+
Prox1+
Sox9-Unsorted
Sox9-Negative
Sox9-Sublow
D
Sox9 -Neg
Sox9 -Sublow
Sox9 -High
Sox9 -Low
Lgr5-High
non-EEC lineage
EEC lineage
miR-7a
miR-7b
miR-215
miR-194
E
RQV (a.u.)
Hopx
Normalized Counts
miR-7
Hopx+
Hopx-
F
RQV (a.u.)
Lgr5
Chga
miR-7
LSP
USP
Lgr5-High
G
RQV (a.u.)
Prox1
Chga
miR-7
Prox1+
Prox1-
H
Prox1+ expression (log2)
log2FoldChange
miR-7
I
Enrichment
miR-7b-5p
miR-375-3p
miR-183-5p+1
miR-183-5p
miR-375-3p+1
miR-375-3p-1
miR-182-5p
let-7e-5p
miR-423-5p
miR-320-3p
J
RQV (a.u.)
Lyz1
Dclk1
miR-7 RQV (a.u.)
Defa6+
Tuft
Sox9-high
Defa6+
Defa6-
Tuft cells
Unsorted

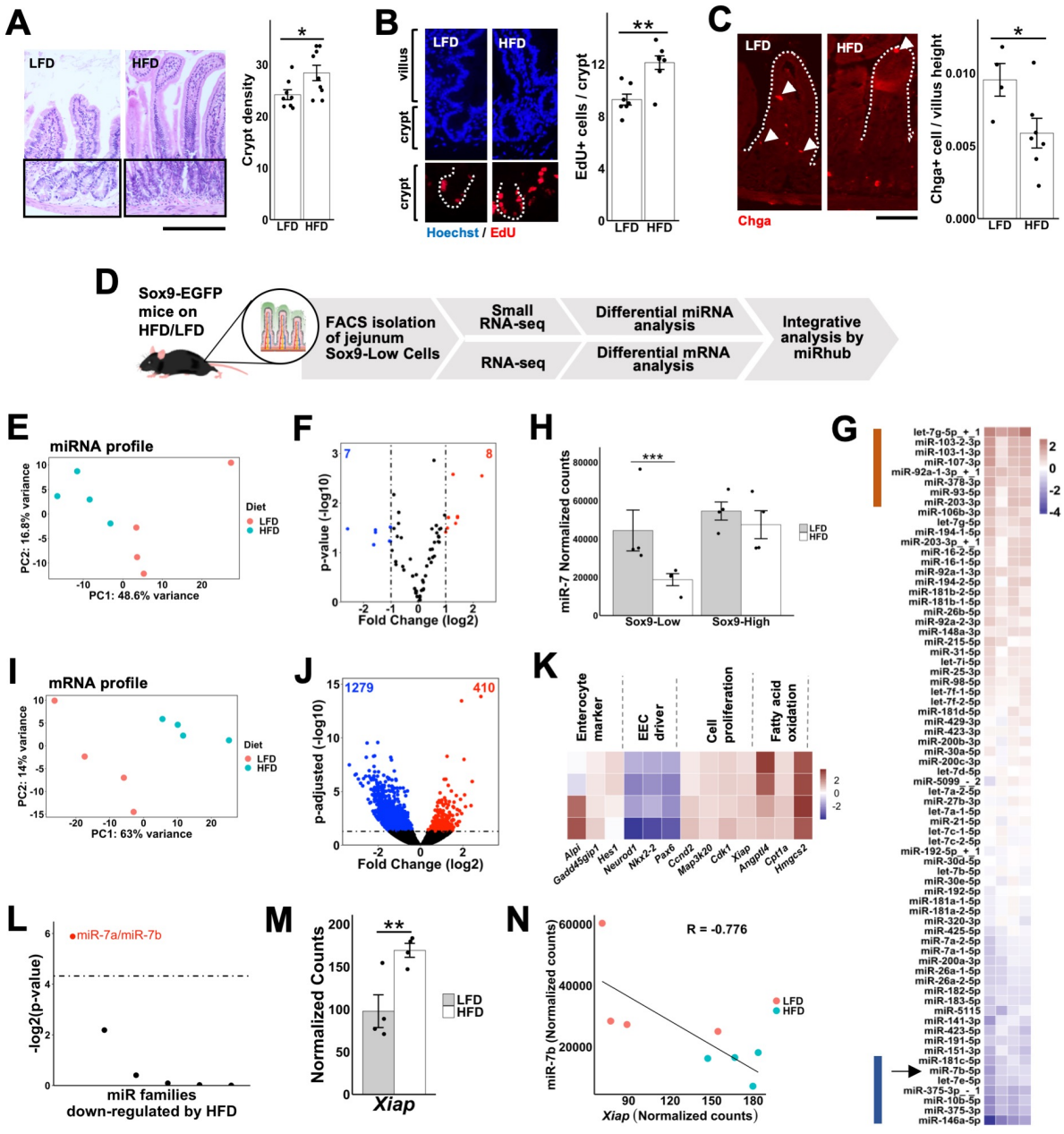
A
LFD
HFD
Crypt density
LFD HFD
B
villus
crypt
crypt
Hoechst / EdU
EdU+ cells / crypt
C
Chga
Chga+ cell / villus height
D
Sox9-EGFP mice on HFD/LFD
FACS isolation of jejunum Sox9-Low Cells
Small RNA-seq
RNA-seq
Differential miRNA analysis
Differential mRNA analysis
Integrative analysis by miRhub
E
miRNA profile
PC2: 16.8% variance
PC1: 48.6% variance
Diet
F
p-value (-log10)
Fold Change (log2)
H
miR-7 Normalized counts
Sox9-Low
Sox9-High
G
I
mRNA profile
PC2: 14% variance
PC1: 63% variance
J
p-adjusted (-log10)
1279
410
Fold Change (log2)
K
Enterocyte marker
EEC driver
Cell proliferation
Fatty acid oxidation
Alpi
Gadd45gip1
Hes1
Neurod1
Nkx2-2
Pax6
Ccnd2
Map3k20
Cdk1
Xiap
Angptl4
Cpt1a
Hmgcs2
L
miR-7a/miR-7b
-log2(p-value)
miR families down-regulated by HFD
M
Normalized Counts
Xiap
N
R = -0.776
miR-7b (Normalized counts)
Xiap (Normalized counts)

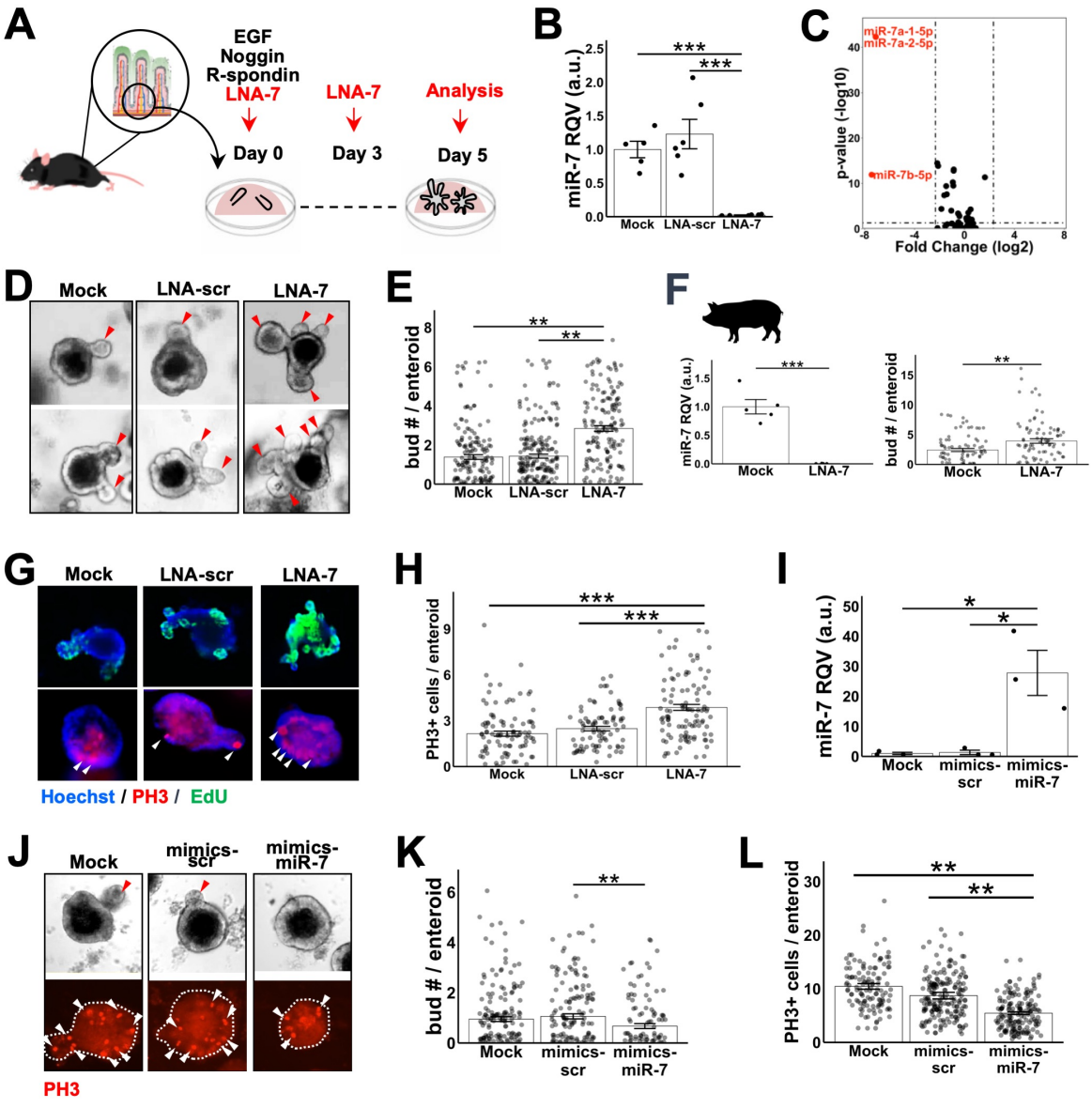
A
EGF
Noggin
R-spondin
LNA-7
Day 0
LNA-7
Day 3
Analysis
Day 5
B
miR-7 RQV (a.u.)
Mock
LNA-scr
LNA-7
C
miR-7a-1-5p
miR-7a-2-5p
miR-7b-5p
p-value (-log10)
Fold Change (log2)
D
Mock
LNA-scr
LNA-7
E
bud # / enteroid
F
miR-7 RQV (a.u.)
bud # / enteroid
G
Mock
LNA-scr
LNA-7
Hoechst / PH3 / EdU
H
PH3+ cells / enteroid
I
miR-7 RQV (a.u.)
mimics-scr
mimics-miR-7
J
Mock
mimics-scr
mimics-miR-7
PH3
K
bud # / enteroid
L
PH3+ cells / enteroid

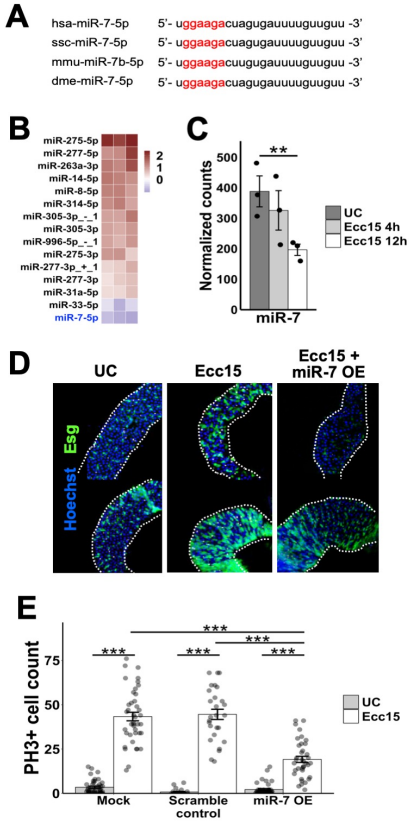

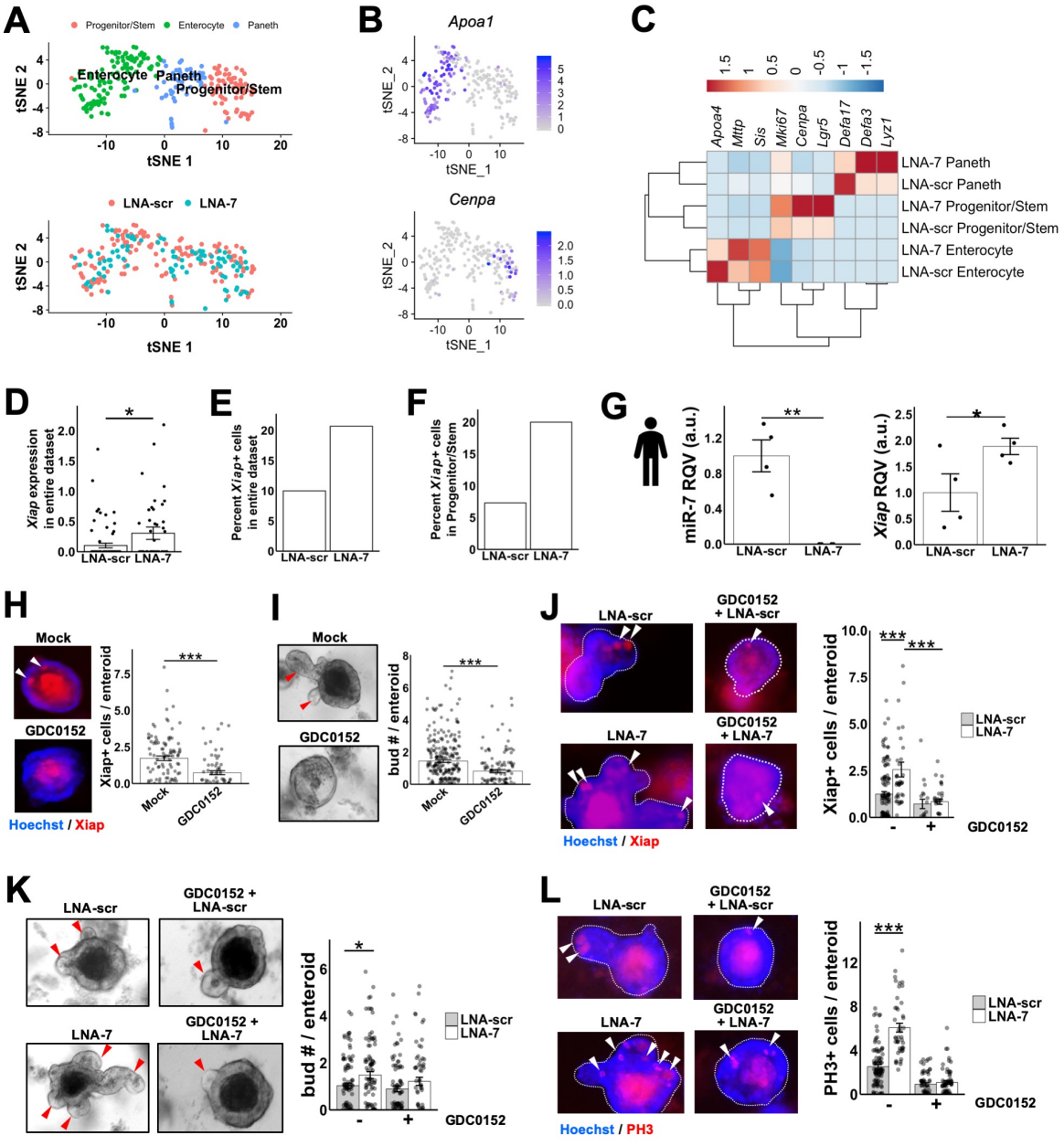
A
Progenitor/Stem
Enterocyte
Paneth
tSNE 2
tSNE 1
LNA-scr
LNA-7
B
Apoa1
Cenpa
tSNE_2
tSNE_1
C
Apoa4
Mttp
Sis
Mki67
Cenpa
Lgr5
Defa17
Defa3
Lyz1
LNA-7 Paneth
LNA-scr Paneth
LNA-7 Progenitor/Stem
LNA-scr Progenitor/Stem
LNA-7 Enterocyte
LNA-scr Enterocyte
D
Xiap expression in entire dataset
E
Percent Xiap+ cells in entire dataset
F
Percent Xiap+ cells in Progenitor/Stem
G
miR-7 RQV (a.u.)
Xiap RQV (a.u.)
H
Mock
GDC0152
Xiap+ cells / enteroid
Hoechst / Xiap
I
bud # / enteroid
J
LNA-scr
GDC0152 + LNA-scr
LNA-7
GDC0152 + LNA-7
K
L
PH3+ cells / enteroid
Hoechst / PH3

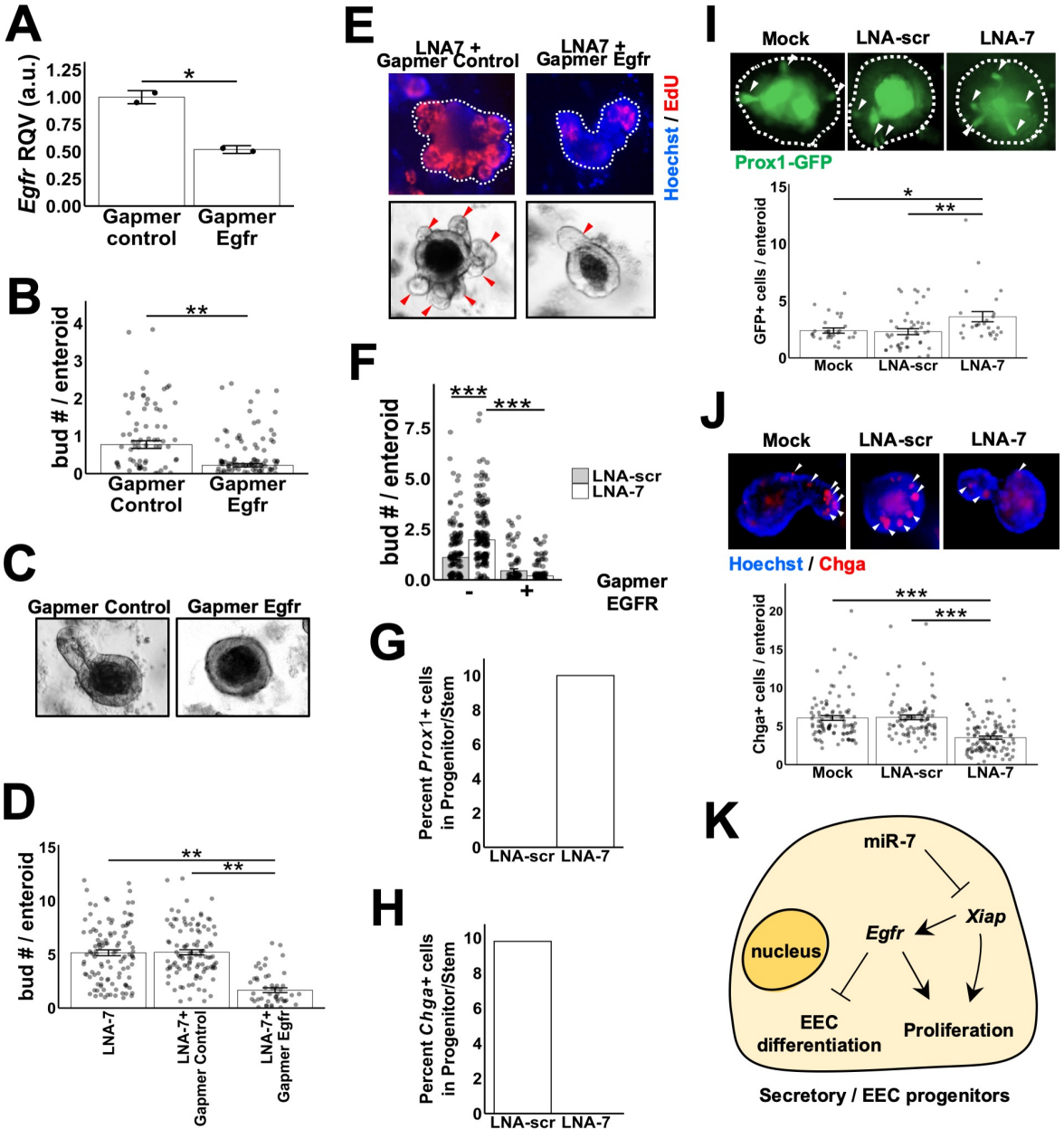
A
Egfr RQV (a.u.)
1.25
1.00
0.75
0.50
0.25
0.00
*
Gapmer control
Gapmer Egfr
B
bud # / enteroid
**
Gapmer Control
Gapmer Egfr
C
Gapmer Control
Gapmer Egfr
D
bud # / enteroid
**
**
LNA-7
LNA-7+ Gapmer Control
LNA-7+ Gapmer Egfr
E
LNA7 + Gapmer Control
LNA7 + Gapmer Egfr
Hoechst / EdU
F
bud # / enteroid
***
***
LNA-scr
LNA-7
Gapmer EGFR
G
Percent Prox1+ cells in Progenitor/Stem
LNA-scr LNA-7
H
Percent Chga+ cells in Progenitor/Stem
LNA-scr LNA-7
I
Mock
LNA-scr
LNA-7
Prox1-GFP
GFP+ cells / enteroid
*
**
J
Mock
LNA-scr
LNA-7
Hoechst / Chga
Chga+ cells / enteroid
***
***
K
miR-7
Xiap
Egfr
nucleus
EEC differentiation
Proliferation
Secretory / EEC progenitors